Research Paper

THEMED ISSUE: Mantle to Surface Dynamics during the Transition from Subduction to Collision to Tectonic Escape: Results from the Continental Dynamics–Central Anatolian Tectonics (CD-CAT) Project

GEOSPHERE

GEOSPHERE, v. 16, no. 6

https://doi.org/10.1130/GES02255.1

15 figures; 1 set of supplemental files

CORRESPONDENCE: paul.umhoefer@nau.edu

CITATION: Umhoefer, P.J., Thomson, S.N., Lefebvre, C., Cosca, M.A., Teyssier, C., and Whitney, D.L., 2020, Cenozoic tectonic evolution of the Ecemiş fault zone and adjacent basins, central Anatolia, Turkey, during the transition from Arabia-Eurasia collision to escape tectonics: Geosphere, v. 16, no. 6, p. 1358–1384, https://doi.org/10.1130/GES02255.1.

Science Editor: Andrea Hampel
Associate Editor: Jason W. Ricketts

Received 10 March 2020
Revision received 19 August 2020
Accepted 17 September 2020

Published online 27 October 2020

Cenozoic tectonic evolution of the Ecemiş fault zone and adjacent basins, central Anatolia, Turkey, during the transition from Arabia-Eurasia collision to escape tectonics

Paul J. Umhoefer[1], Stuart N. Thomson[2], Côme Lefebvre[3], Michael A. Cosca[4], Christian Teyssier[3], and Donna L. Whitney[3]

[1]School of Earth and Sustainability, Northern Arizona University, Flagstaff, Arizona 86011, USA
[2]Department of Geosciences, University of Arizona, Tucson, Arizona 85721, USA
[3]Department of Earth & Environmental Sciences, University of Minnesota, Minneapolis, Minnesota 55455, USA
[4]U.S. Geological Survey, Denver Federal Center, MS 963, Denver, Colorado 80225, USA

ABSTRACT

The effects of Arabia-Eurasia collision are recorded in faults, basins, and exhumed metamorphic massifs across eastern and central Anatolia. These faults and basins also preserve evidence of major changes in deformation and associated sedimentary processes along major suture zones including the Inner Tauride suture where it lies along the southern (Ecemiş) segment of the Central Anatolian fault zone. Stratigraphic and structural data from the Ecemiş fault zone, adjacent NE Ulukışla basin, and metamorphic dome (Niğde Massif) record two fundamentally different stages in the Cenozoic tectonic evolution of this part of central Anatolia. The Paleogene sedimentary and volcanic strata of the NE Ulukışla basin (Ecemiş corridor) were deposited in marginal marine to marine environments on the exhuming Niğde Massif and east of it. A late Eocene–Oligocene transpressional stage of deformation involved oblique northward thrusting of older Paleogene strata onto the eastern Niğde Massif and of the eastern massif onto the rest of the massif, reburying the entire massif to >10 km depth and accompanied by left-lateral motion on the Ecemiş fault zone. A profound change in the tectonic setting at the end of the Oligocene produced widespread transtensional deformation across the area west of the Ecemiş fault zone in the Miocene. In this stage, the Ecemiş fault zone had at least 25 km of left-lateral offset. Before and during this faulting episode, the central Tauride Mountains to the east became a source of sediments that were deposited in small Miocene transtensional basins formed on the Eocene–Oligocene thrust belt between the Ecemiş fault zone and the Niğde Massif. Normal faults compatible with SW-directed extension cut across the Niğde Massif and are associated with a second (Miocene) re-exhumation of the Massif. Geochronology and thermochronology indicate that the transtensional stage started at ca. 23–22 Ma, coeval with large and diverse geological and tectonic changes across Anatolia.

Paul J. Umhoefer https://orcid.org/0000-0002-6538-3335

1. INTRODUCTION

Intracontinental deformation associated with collision commonly leads to the development of large, lithosphere-scale, strike-slip fault systems and associated basins and exhumed crystalline massifs. Examples of major strike-slip systems occur in Anatolia (north and east Anatolian fault zones; e.g., Hempton, 1982), many faults in the Alps (e.g., Selverstone, 1988; Ratschbacher et al., 1991), the North American Cordillera (e.g., Gabrielse, 1985; Coleman and Parrish, 1991), the Appalachians and Caledonides (Chauvet and Séranne, 1994; Dewey and Strachan, 2003), and the Himalaya-Tibet orogenic system (e.g., Peltzer and Tapponnier, 1988; Yin et al., 2002). Significant questions about the development of these fault systems relate to their locations (i.e., why they form where they do), length, displacement (vertical and/or lateral), timing of inception relative to collision, seismic behavior, relation to topography, and role in strain localization through time. The behavior of lithosphere-scale, intracontinental fault systems also plays a role in the interaction of the upper and lower crust, and the crust and upper mantle, including the degree of decoupling and crust and/or mantle strength (rheology).

An important aspect of the evolution of these strike-slip fault zones is their role in significant vertical displacement of the crust. Episodes of burial and exhumation along intracontinental strike-slip faults may record displacement along steps and bends in the fault system (Wilcox et al., 1973; Crowell, 1974; Sylvester, 1988) and/or the response of the fault system to changes in the far-field tectonic regime. Although multiple cycles of burial and exhumation (yo-yo tectonics: Umhoefer et al., 2007) along strike-slip faults are not as large in magnitude (changes in depth) as those in subduction and collision zones (e.g., Rubatto et al., 2011), burial and exhumation may be on the scale of a few to tens of km and therefore have a structural and petrologic and/or geochemical effect that can be discerned from field observation of structures and basins, from petrographic analysis of mineral assemblages and microstructures, and analysis of mineral thermochronometers (Umhoefer et al., 2007; Whitney et al., 2008). That is, the depth-temperature-time history can be determined in the context of particular structures involved in the vertical displacements, and

related to changes in the tectonic regime, such as switches from transpression to transtension in a strike-slip fault zone.

Many complex collision zones feature suture zones where ocean basins have closed. One of these suture zones within the Anatolian plate (Figs. 1 and 2) is the Inner Tauride suture zone, the boundary between the Anatolide-Tauride belt to the south (Tauride Mountains) and the Central Anatolian crystalline complex (CACC), or Kırşehir block, to the northeast (Fig. 2). An excellent example of a lithosphere-scale, strike-slip fault system that has formed along a suture zone is the Ecemiş fault zone, which is the southern segment of the Central Anatolian fault zone in Turkey (Toprak and Göncüoğlu, 1993; Koçyiğit and Beyhan, 1998) (Fig. 1). The Ecemiş fault zone, which experienced both large-magnitude horizontal and vertical motion, formed along the SE boundary of the CACC and the Inner Tauride suture zone.

The Ecemiş fault zone is adjacent to the Niğde Massif (Fig. 2), a part of the CACC that records two episodes of burial and exhumation driven by a switch from transpression to transtension (Umhoefer et al., 2007; Whitney et al., 2007, 2008; Idleman et al., 2014). Although the timing of this "yo-yo" tectonic history has been documented within and along the eastern edge of the Niğde Massif (Umhoefer et al., 2007), the structures, and therefore the mechanisms responsible for the burial and exhumation cycles, have not previously been identified, and the history of the basin ("Ecemiş corridor" herein) between the Niğde Massif and Ecemiş fault zone has not been integrated with that of the Niğde Massif.

In this paper, we present new observations and data of oblique thrust faults and related structures that we propose were responsible for the Eocene–Oligocene transpressional burial stage, new structural and stratigraphic data on the Miocene transtensional stage, and geochronology and thermochronology data for the sedimentary basin of the Ecemiş corridor, to track the thermal effects of transpression and the timing of the subsequent transtensional faulting, exhumation, and sedimentation. We then briefly relate this two-stage deformation-basinal history of the Ecemiş corridor and fault zone to regional tectonic events, including Arabia-Eurasia collision.

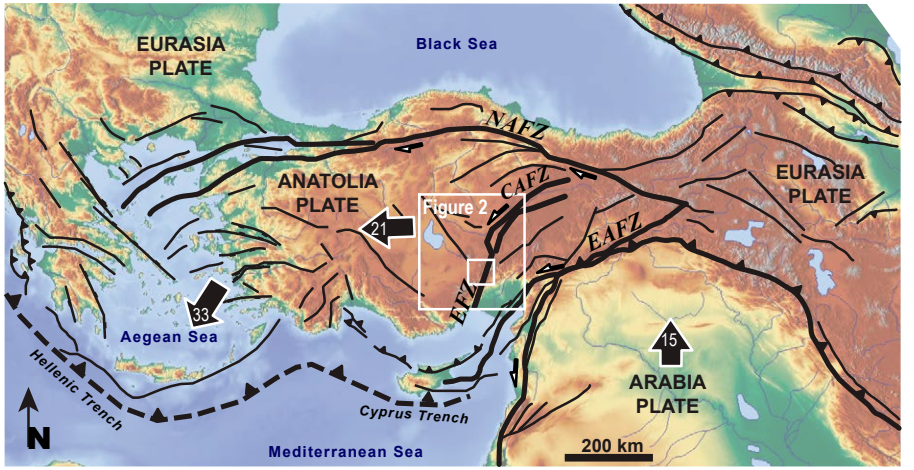

Figure 1. Tectonic and digital shaded relief map of the Eastern Mediterranean orogenic system showing plate boundaries (thick black lines) and some of the main faults (black) of the region. Arrows indicate GPS-derived, Eurasia-fixed relative plate motion in mm/yr (Reilinger et al., 2006). The white box within the area of Figure 2 is Figure 3 and the study area. NAFZ—North Anatolian fault zone; EAFZ—East Anatolian fault zone; CAFZ—Central Anatolian fault zone; EFZ—Ecemiş fault zone.

2. GEOLOGICAL SETTING

Fundamentally, Anatolia formed as a result of the closure of the Paleotethys and Neotethys Oceans in the Mesozoic and Cenozoic (Şengör, 1984). Suture zones from the Neotethys closing are the Izmir-Ankara-Erzincan suture zone in the north (Fig. 2), the Inner Tauride suture zone co-located with the latter in the east and in the west wrapping around the southern margin of the CACC (Fig. 2), and the Bitlis suture zone along the northern margin of the Arabia plate (Fig. 1). Widespread evidence supports a latest Cretaceous to early Paleocene collision of the Anatolide-Tauride blocks and CACC with the Pontides block to form the Izmir-Ankara-Erzincan suture zone and closure of the northern Neotethys (e.g., Yılmaz et al., 1997; Okay and Tüysüz, 1999; Kaymakcı et al., 2009; Meijers et al., 2010; Parlak et al., 2013).

The timing of Arabia-Eurasia collision and its relation to the Inner Tauride suture zone is controversial, and estimates range from Eocene to Miocene. Interpretations of Eocene- or Oligocene-age collision involve "soft" collision between the outer passive margin of Arabia and Eurasia (Anatolide-Tauride block) and are partly based on deformation across much of Anatolia (e.g., Hempton, 1987; Yılmaz, 1993; Jolivet and Faccenna, 2000; Rolland et al., 2012; McQuarrie and van Hinsbergen, 2013; Ballato et al., 2018; Darin et al., 2018). The younger collision models emphasize the history of the Bitlis suture zone during the early to middle Miocene (Şengör and Yılmaz, 1981; Okay et al., 2010; Cavazza et al., 2018; Darin and Umhoefer, 2019).

The central Anatolian region is in an intermediate position between the zone of collision in the east and a zone of extension in western Turkey and the Aegean Sea region. Major geologic features of central Anatolia are (Figs. 1 and 2):

(1) the Central Anatolian fault zone (Koçyiğit and Beyhan, 1998), including the southern (Ecemiş) segment that is discussed in this

paper (e.g., Jaffey and Robertson, 2001; Umhoefer et al., 2007; Higgins et al., 2015; Yıldırım et al., 2016);

(2) the central segment of the Tauride Mountains (uplifted since the Miocene; Cosentino et al., 2012; Schildgen et al., 2012a, 2012b; Meijers et al., 2018); this segment is part of the Anatolide-Tauride belt;

(3) a series of metamorphic and plutonic massifs that represent the Late Cretaceous orogenic crust of the CACC (Akıman et al., 1993), including the Niğde Massif, which is part of the focus of this study (Göncüoğlu, 1982; Whitney et al., 2001, 2003);

(4) fragments of Late Cretaceous ophiolites that lie on the CACC and the Anatolide-Tauride belt (e.g., Yalınız et al., 1996; Vergili and Parlak, 2005; van Hinsbergen et al., 2016; Radwany et al., 2017, 2020);

(5) large sedimentary basins formed from the Late Cretaceous through the Cenozoic (e.g., from east to west the Sivas, Ulukışla, and Tuz Gölü basins) (Cater et al., 1991; Clark and Robertson, 2002; Gürer et al., 2016, 2018; Darin et al., 2018), across the time period of debate on the timing of collision of Arabia; and

(6) the Cappadocian volcanic province (Miocene to present) (e.g., Le Pennec et al., 1994; Aydar et al., 1995; Dhont et al., 1998; Temel et al., 1998; Reid et al., 2017).

The entire Central Anatolian fault zone is >700 km long and extends from the Mediterranean Sea to the eastern end of the North Anatolian fault, with a prominent bend or step in central Anatolia at the Erciyes volcano (Fig. 2). The Ecemiş (southern) fault segment experienced ~60 km (Jaffey and Robertson, 2001) to 80 km (Koçyiğit and Beyhan, 1998) of left-lateral displacement. From the late Eocene to the mid-late Miocene, displacement was largely left-lateral and then became more transtensional and/or extensional in the late Miocene–early Pliocene (Jaffey and Robertson, 2001), and finally a down-to-the-west normal fault in the Quaternary (Higgins et al., 2015). The origin of the fault may have been related to oblique convergence during closure of the Neotethys seaway in this region (Clark and Robertson, 2005; Umhoefer et al., 2007).

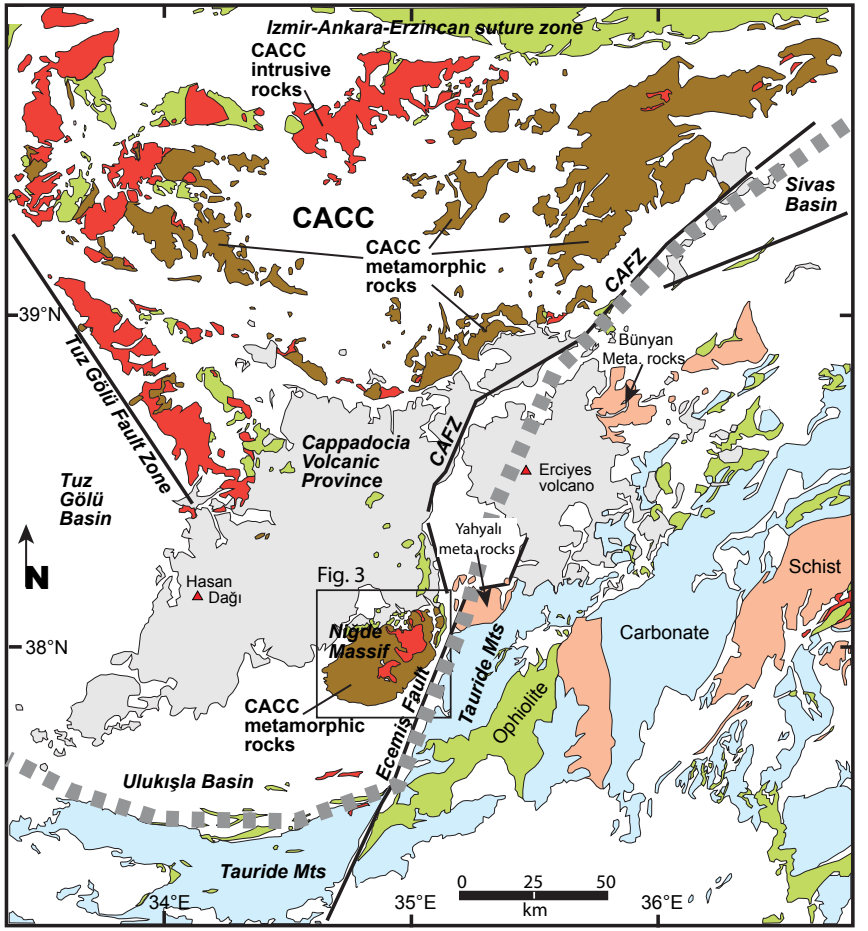

Figure 2. Simplified geologic map of the region surrounding the study area (Fig. 3) emphasizing the older belts and the Neogene Cappadocia volcanic province in gray. Areas in white are Cenozoic basins and Quaternary deposits. The Central Anatolian crystalline complex (CACC) comprises the metamorphic (brown) and plutonic rocks (red) of the triangular block west of the Central Anatolian fault zone (CAFZ), also known as the Kırşehir block. The Inner Tauride suture zone (wide dashed gray line) runs through the study area from the Sivas basin on the northeast south along the Ecemiş fault zone and then west along the northern side of the Tauride Mountains.

The orogenic middle crust represented by the Niğde Massif experienced transpression in the Late Cretaceous (Whitney et al., 2003, 2007) and was partially exhumed by extension (Whitney and Dilek, 1997) or transtension (Whitney et al., 2007) and erosion (Gautier et al., 2002). The Niğde Massif is a structural dome defined by outward-dipping foliation and lithologic layering of metasedimentary rocks and minor amphibolite. Lineation is shallow and trends NE-SW in the high-grade core of the massif (Whitney et al., 2007). The highest grade rocks (including migmatite) are in the core of the

massif (Whitney and Dilek, 1998; Whitney et al., 2001). Peak (sillimanite zone) metamorphism and crystallization of partial melt and granite have been dated at ca. 92 Ma (U-Pb zircon) (Whitney et al., 2003). The youngest U-Pb monazite ages (range of 90–80 Ma) from high-grade metamorphic rocks and granite overlap with hornblende $^{40}Ar/^{39}Ar$ ages (81–79 Ma); $^{40}Ar/^{39}Ar$ ages for biotite, muscovite, and K-feldspar indicate rapid Late Cretaceous cooling at ca. 69 Ma (Whitney et al., 2003). Abundant normal-sense shear zones that record amphibolite- to greenschist-facies conditions are evidence that this exhumation was driven largely by extension (Whitney and Dilek, 2001; Whitney et al., 2007). The Niğde Massif was onlapped by Paleocene–Eocene sedimentary deposits, then reburied, reheated, and deformed in the middle Eocene to Oligocene, and exhumed again in the Miocene (Umhoefer et al., 2007). This cycle of burial and exhumation is part of the focus of the present study.

The presence of metamorphic and plutonic clasts from the Niğde Massif in directly overlying Paleocene–Eocene conglomerate (Umhoefer et al., 2007) from the Çamardı Formation demonstrates that the massif was exposed at Earth's surface. The presence of early Cenozoic marine to marginal marine sedimentary rocks of the Evliyatepe Formation (including the interfingering conglomerates of the Çamardı Formation) overlying the massif across a nonconformity indicates that exposure occurred by ca. 60–50 Ma. The sedimentary rocks were later deformed and metamorphosed to greenschist facies near the massif (Umhoefer et al., 2007). The contact between the metamorphic and/or plutonic rocks and (meta)sedimentary cover is in places a low-angle (~30°) normal fault (Whitney and Dilek, 1997) and in places a sheared nonconformity (Gautier et al., 2002; Umhoefer et al., 2007). The reburial and/or reheating episode postdated deposition of early to middle Eocene nummulitic limestone (Göncüoğlu et al., 1991) in the deformed sedimentary sequence and predates Miocene fission-track cooling ages from detrital apatite that was reset by burial and/or heating (Umhoefer et al., 2007). Maximum heating during this episode of burial has been dated at ca. 30 ± 5 Ma by K-feldspar multidomain diffusion modeling of metamorphic rocks at the eastern margin of the Niğde Massif (Idleman et al., 2014), with final exhumation to the surface sometime after ca. 25 Ma (Fayon et al., 2001; Idleman et al., 2014). Based in part on the presence of disorganized lineations in the eastern part of the massif (compared to the well-organized mineral lineations in the core region) and the coincidence of this region with disturbed $^{40}Ar/^{39}Ar$ ages, Whitney et al. (2007) proposed dividing the Niğde Massif into western and eastern belts separated by a zone of locally intense deformation. The nature of the boundary zone between the eastern and western (core) belts and its relationship to the metamorphic-tectonic history of the area remain poorly understood (Fig. 3).

The Cenozoic sedimentary rocks that overlie the Niğde Massif are part of a narrow basin (2–8 × 30 km) formed between the massif and the Ecemiş fault zone; this basin is the NE extension of the Ulukışla basin (Clark and Robertson, 2002; Gürer et al., 2016). However, the exposed Ecemiş corridor sedimentary rocks consist of only Cenozoic-age strata, while the main Ulukışla basin includes Upper Cretaceous and Cenozoic strata (Gürer et al., 2016). Strata of the Ecemiş corridor were deposited on the Niğde metamorphic rocks in the west and the Mesozoic rocks of the Tauride Mountains in the east within the Ecemiş fault zone (Fig. 3).

3. STRATIGRAPHY OF THE ECEMIŞ CORRIDOR (NE ULUKIŞLA BASIN)

The stratigraphy and depositional environments of the Ecemiş corridor are summarized here mainly from previous studies (Göncüoğlu et al., 1991; Yetiş et al., 1995; Jaffey and Robertson, 2001, 2005; Clark and Robertson, 2002; Umhoefer et al., 2007; Gürer et al., 2016; Meijers et al., 2016) with a few new observations from our mapping. In the sections below, we augment this stratigraphic summary with our new structural mapping and analysis and new thermochronology and geochronology data to reveal new information that adds critical aspects to the overall stratigraphic record of the Ecemiş corridor. Our mapping and structural analysis clarify the contacts of many units in the area.

The main Ulukışla basin to the south of the Ecemiş corridor consists of three sequences bounded by unconformities (Gürer et al., 2016). The lower sequence of Upper Cretaceous (Campanian) to Paleocene age consists of deep marine siliciclastics and carbonates overlain by marine volcanic rocks interbedded with volcaniclastics and limestones. The Eocene middle sequence includes variable deep to shallow marine limestone and turbidites locally capped by evaporites. The upper Oligocene to Miocene upper sequence is exposed in local subbasins, lies on a major unconformity, and consists of terrestrial clastic rocks with interbedded limestones and gypsum deposited in streams and lakes (Jaffey and Robertson, 2005; Meijers et al., 2016).

The *Ulukışla Formation* (Fig. 3) consists of 1500–2000 m of marine volcanic breccias and conglomerates, lavas, volcaniclastic rocks, and minor interbedded marine fossiliferous limestones (Gürer et al., 2016). Locally, the unit includes a sedimentary section of marl, shale, and sandstone with the more prominent fossiliferous limestone. In the northern part of the main basin, the age of the Ulukışla Formation is constrained near its base by a 59.7 Ma welded tuff and 59.6 Ma rhyolite lava, both dated by U-Pb zircon; a welded tuff at the top of the unit in the central basin yielded a U-Pb zircon age of 56.9 Ma (Gürer et al., 2016). In the Ecemiş corridor, the base of the Ulukışla Formation is not exposed, and the unit forms a thrust nappe through the center of the area (Fig. 3).

Gürer et al. (2016) interpreted that the *Çamardı Formation* underlies and interfingers with the Ulukışla Formation volcanic rocks across the basin, whereas in the Ecemiş corridor, we restrict the Çamardı Formation to the narrow belt along the Niğde Massif. The Çamardı Formation has Late Cretaceous to late Paleocene nannofossils in the main Ulukışla basin; these nannofossils progressively become younger from west to east (Gürer et al., 2016), in agreement with a Paleocene age assignment from earlier workers for the Ecemiş corridor (Göncüoğlu et al., 1991; Yetiş et al., 1995). In the Ecemiş corridor, the unit consists of up to 120 m of marginal to shallow marine conglomerate, sandstone, and minor fine-grained clastic rocks deposited on and near the Niğde Massif (Umhoefer

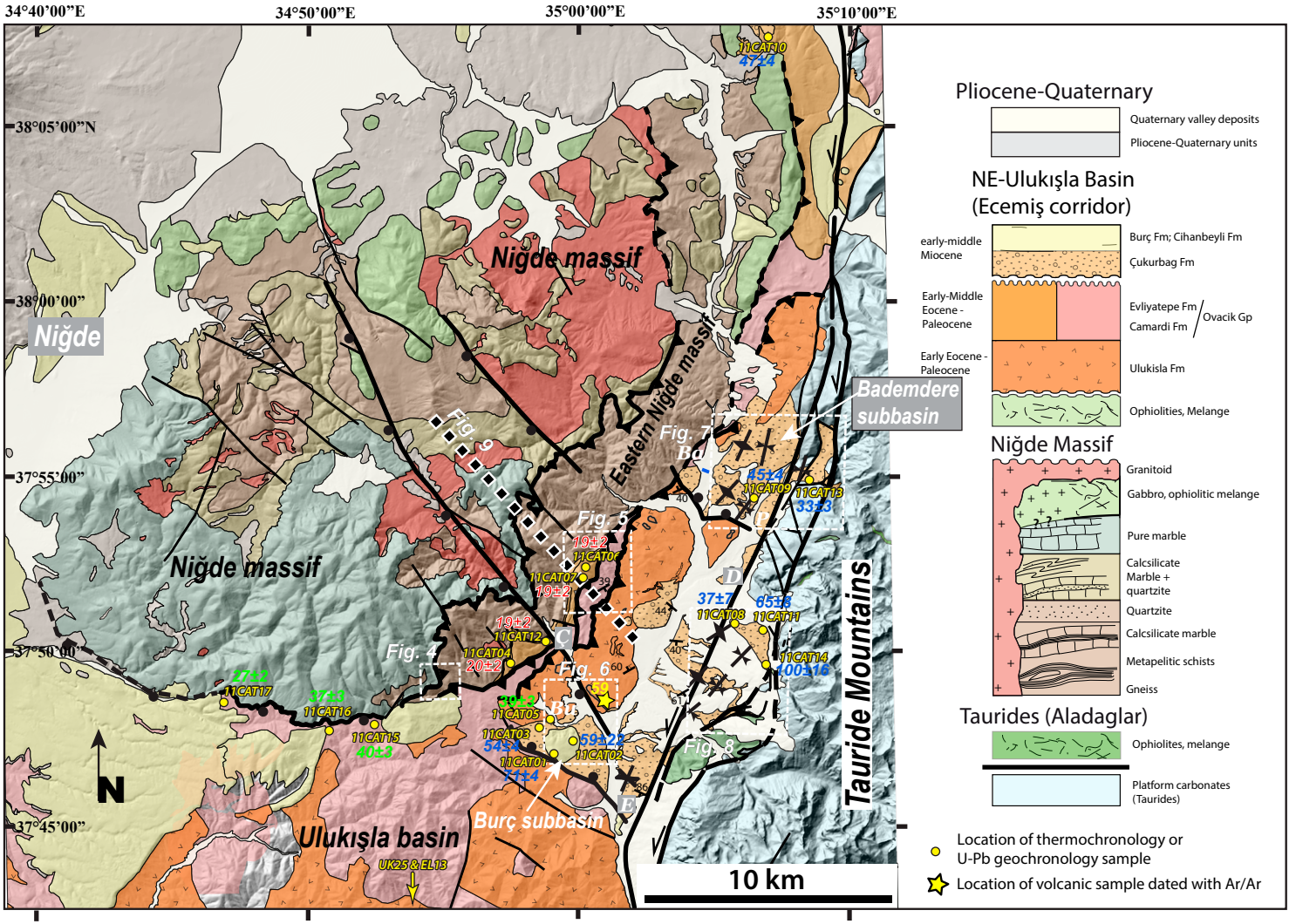

Figure 3. Geologic map and tectonostratigraphic columns of the Niğde-Çamardı-Ecemiş fault zone study area with the Niğde Massif to the west, Tauride Mountains to the east, and the northeastern Ulukışla basin (Ecemiş corridor) between them. The Ecemiş fault zone is the left lateral fault zone on the western edge of the Tauride Mountains. Dotted white rectangles indicate location of detailed maps presented in Figures 4–8. Dotted thick black line indicates the trace of the cross section of Figure 9. The red, green, and blue ages adjacent to the yellow sample numbers are the apatite fission-track ages as interpreted on Figure 13 and in the text as cooling ages, partially reset ages, and detrital ages, respectively. The 59 Ma age in yellow next to the yellow star is the $^{40}Ar/^{39}Ar$ age. White abbreviations are the villages of Ba—Bademdere, Bu—Burç, Ç—Çamardı, D—Demirkazık, E—Elekgölü, P—Pinarbaşı. The large city of Niğde is on the left.

et al., 2007). We reinterpret a narrow thrust nappe immediately to the east of the belt of Çamardı Formation as the Ovacık Group (Fig. 3).

The upper Çamardı Formation along the Niğde Massif underlies and interfingers with the *Evliyatepe Formation* (Göncüoğlu et al., 1991; Umhoefer et al., 2007), a 200–300-m-thick unit of marine limestone, sandstone, marl, and minor conglomerate; this unit changes upsection from a deltaic environment to an open, shallow marine environment. Based on marine fossils, the Evliyatepe Formation was assigned to the early to middle Eocene (Göncüoğlu et al., 1991; Gautier et al., 2002) and correlates with the shelfal limestones of the middle Eocene Hasangazi Formation in the southern Ulukışla basin (Clark and Robertson, 2002). Gürer et al. (2016) included the Evliyatepe Formation in the Hasangazi Formation and part of the Ovacık Group.

Our mapping shows that the belt of Çamardı and Evliyatepe formations rocks along the east side of the Niğde Massif was thrust under the Ovacık Group (Fig. 3), and therefore the stratigraphic relation between these units is unknown. However, based on known ages and depositional environments, we interpret the Çamardı and Evliyatepe formations as marginal to shallow marine equivalents of the deeper marine volcanic and sedimentary rocks of the Ulukışla and Ovacık units. Probable Eocene foraminifera-bearing limestones and marls exposed in a few 100-m-scale fault blocks within the Ecemiş fault zone are correlated with the Evliyatepe Formation or Ovacık Group based on lithologies.

The *Ovacık Group* overlies the Ulukışla Formation and comprises mixed marine clastic and carbonate units of early to middle Eocene age (Clark and Robertson, 2002); these units have been proposed by Gürer et al. (2016) to include the Hasangazi and Bolbeztepe formations. In the southern Ulukışla basin, the Kabaktepe Formation (Clark and Robertson, 2002, 2005) conformably overlies the Ovacık Group and consists of anhydrite, gypsum, dolomite, and sandstone with microfossils of late Lutetian age.

A nearly continuous belt of Ovacık Group rocks runs along the west side of the Ecemiş corridor and forms a thrust nappe where mapped in the most detail (Fig. 3). Here the rocks of the Ovacık Group consist of thin-bedded gray marl, variably colored (mainly black to red) shale, and minor thick-bedded limestone. Foraminiferal limestone and marl fault blocks within the Ecemiş fault zone suggest that the Ovacık Group was deposited on top of the Ulukışla Formation from the Niğde Massif in the west to the Tauride platform in the east during early to middle Eocene time.

The entire Ulukışla basin records a major late Eocene to late Oligocene unconformity that spans from ca. 40–27 Ma in the main basin and from ca. 40 to ca. 25 Ma in the Ecemiş corridor. The end of marine deposition was at ca. 40 Ma (Lutetian), and the beginning of terrestrial deposition was in the late Oligocene with the formation of three local subbasins within the greater Ulukışla basin: the Aktoprak Formation in a syncline in the southern Ulukışla basin (Gürer et al., 2016; Meijers et al., 2016); the Bademdere subbasin (Jaffey and Robertson, 2005; this study) of the Çukurbağ Formation in the northern study area (Fig. 3); and the Burç subbasin (and Burç Formation) in the southern study area (Jaffey and Robertson, 2005; Gürer et al., 2016). In these subbasins, the terrestrial Aktoprak and Çukurbağ formations unconformably overlie the older marine strata and Mesozoic rocks of the Tauride belt. The Aktoprak Formation consists of ~900 m of lacustrine marls and limestones overlain by fluvial red-green clastic sandstones and blue-gray marls (Jaffey and Robertson, 2005). Meijers et al. (2016) concluded based on magnetostratigraphy of the lower ~300 m of the unit that it was deposited in the Chattian (from 27.1 to 24.7 Ma), and therefore the upper part of the unit is latest Oligocene to Miocene. Extrapolating the sedimentation rates from the lower section would suggest that deposition of the Aktoprak Formation continued to ca. 20 Ma or near the end of the Aquitanian, in agreement with Chattian–Aquitanian gastropods and ostracods (Meijers et al., 2016).

Jaffey and Robertson (2005) described the *Çukurbağ Formation* in the Ecemiş corridor as an ~1000 m composite section in the Bademdere area where it is thickest, and our observations and mapping confirm their results. The Çukurbağ Formation remains undated by direct evidence, until this study (summarized below). The unit consists of a base of calcareous mudstones incised by fluvial channels of limestone pebble to cobble conglomerate locally overlain by microbial carbonates deposited in a floodplain with local small lakes and marshes. The middle of the unit is mainly red sandstones and mudstones with increasing conglomerates upward deposited in braided streams and floodplains. The upper part of the unit consists of calcareous mudstones interbedded with sandstones and micritic limestones with minor silty coals locally overlain by an interval of gypsum and anhydrite breccia deposited in a carbonate lake that becomes evaporitic upward (Jaffey and Robertson, 2005). Stable isotopes showed that some of the small lakes were hydrologically open basins (Lüdecke et al., 2013).

From our study in the Bademdere subbasin, we determined that (1) the lower carbonate changes laterally to the southeast into fluvial red beds and conglomerates; (2) the lower section is capped by gypsum that is up to 50 m thick in the west and limestone-clast conglomerate to the east; and (3) the upper section is mainly a thick-striped red and gray sandstone and mudstone overlain locally by the carbonate and evaporite lake deposits. More marginal areas of the Çukurbağ Formation, especially near and within the Ecemiş fault zone, have more conglomerates with subrounded clasts up to boulder size and dominated by limestone clasts mainly derived from the Mesozoic Tauride platform, but with a minor component of Eocene limestone clasts. Other minor clasts across the Çukurbağ belt are volcanics (mainly andesites correlated to the Ulukışla Formation), sandstone, gabbro, and rare granite, marble, ultramafics, and quartzite. Locally the gabbro clasts are common. Based on geochemical analysis of 17 gabbro clasts, Radwany et al. (2017) suggested that the Çukurbağ conglomerates were partly derived from the Tauride ophiolites and from an unmetamorphosed or low-grade part of the central Anatolian ophiolite, which may have covered much of the Niğde Massif in Oligocene–early Miocene time. Paleocurrent data (Jaffey and Robertson, 2005) and the facies patterns suggest that the subbasins of the Çukurbağ Formation were elongate and inward-draining along the Ecemiş

corridor with the Bademdere subbasin, the largest depocenter in the study area. About 4 km NNE of the city of Çamardı is a small half graben of mainly gypsum lying over and faulted against the thrust nappe of the Ovacık Group (Fig. 3).

The *Burç Formation* is only exposed in the Ecemiş corridor and in its type location (Burç subbasin near the village of Burç and 4–5 km south of Çamardı, Fig. 3) is a ~140 m section of fine-grained limestone (marl), microbial limestone, minor coal and tufa, and meter-scale cross-bedded sandstones up to 3 m thick (Jaffey and Robertson, 2005). The Burç Formation in its type location has been interpreted to be middle to late Miocene age based on gastropods (Yetiş, 1968). The unit has common plant fragments, gastropods, and ostracods (Yetiş, 1968), which, together with the lithofacies, indicate that it was deposited in a lake interrupted by streams in the middle to upper part of the section. Paleocurrents from the crossbedded stream channels show that the streams were flowing to the east and SE toward the Ecemiş fault zone (Jaffey and Robertson, 2005). The unit conformably overlies the Çukurbağ Formation in the type area, and we interpret that the Burç Formation is equivalent to the upper lacustrine facies of the Çukurbağ Formation in the Bademdere subbasin.

At the top of the Ulukışla Basin, the *Cihanbeyli Formation* unconformably overlies Paleogene and Miocene rocks south of the Niğde Massif and is composed of late Miocene lacustrine sediments interbedded with volcanic tuff and fluvial conglomerate (MTA map, 2002); this unit records major drainage changes in the late Miocene to Quaternary (Radwany et al., 2017); these changes postdate the events discussed in the present study. The Cihanbeyli Formation is dated as late Miocene from 6 to 7 Ma tuffs (Meijers et al., 2018).

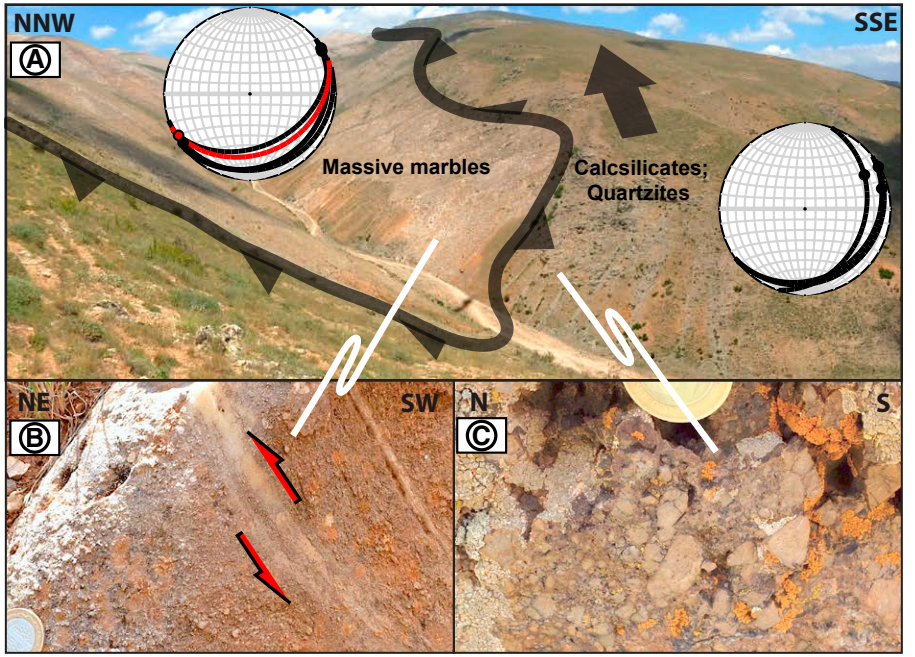

Figure 4. Interpreted field photographs (A–C) and structural data (foliation and fault surfaces) on stereonets (A) from near the thrust fault in the Celallar area that places the eastern belt of the Niğde Massif over the core of the massif. Photographs by Côme Lefebvre.

4. STRUCTURE OF THE ECEMIŞ CORRIDOR IN THE NIĞDE-ÇAMARDI AREA

This section summarizes the results of local detailed mapping and structural analysis along the ~20 km of the Ecemiş corridor (Figs. 4–8), including observations at outcrop to microstructural scales and a cross section that illustrates key fault relations (Fig. 9). Mapping included two parts of the Ecemiş fault zone (Figs. 7 and 8) and much of the eastern belt of the Niğde Massif (Figs. 3–5), as well as many areas between the Ecemiş fault zone and massif.

The mapping and structural analysis indicate that there were two stages of deformation that produced distinct structural patterns at the kilometer scale; we summarize those patterns here before providing local evidence for these conclusions in each section below. Older stage 1 structures include three thrust nappes that overlie NNE-striking thrust faults mapped along the Ecemiş corridor (Fig. 3). The western thrust fault displaced metamorphic rocks of the eastern belt of the Niğde Massif over the core of the massif, with local structures indicating oblique, northward motion as documented below from the Cellaler area (Fig. 4). To the east, the Ovacık Group is thrust over the eastern belt, and the Ulukışla Formation is thrust over the Ovacık Group, and both thrust faults show oblique northward kinematics. The Ovacık thrust nappe has a narrow (200–300 m) belt of Ulukışla volcanic rocks at its base from ~3 km north of Çamardı and northward. Given the length of these thrust faults, they likely continue into the northern part of the map area (Fig. 3), though they were not mapped in detail there.

The stage 2 deformation includes two large NW-SE–striking normal faults that are mapped through much or all of the Niğde Massif and that may cut through the Ecemiş corridor (Fig. 3). The normal fault at the southern boundary of the Niğde Massif has a similar orientation, as do many faults within the Ecemiş fault zone. These normal faults

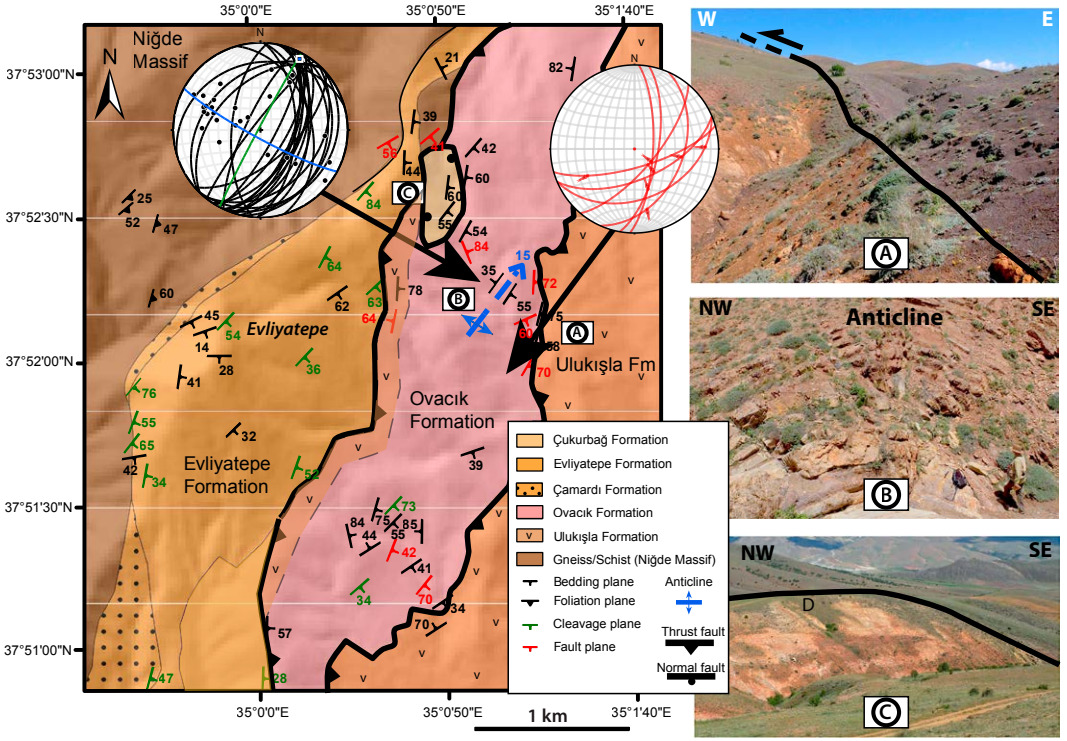

Figure 5. Detailed geologic and tectonic map of the NE Evliyatepe area, including interpreted field photographs and structural data from bedding planes (black on stereonet), foliation, and fault surfaces (red on stereonet) from one well-exposed traverse. Photographs A–C are from locations on the map. Photographs by Côme Lefebvre.

cut the oblique thrust faults and the Çukurbağ and Burç formations. NW-striking, down-to-the-NE normal faults are likely to bound the southern edges of the Burç and Bademdere subbasins, and strata of each subbasin are broadly folded into open synclines and anticlines trending subparallel to a little more easterly than the Ecemiş fault zone (Fig. 3). A discontinuous belt of outcrops of the Çukurbağ Formation lies along the eastern edge of the Ecemiş corridor adjacent to the Ecemiş fault zone and connects the subbasins. Within this Çukurbağ belt and >100 to ~500 m west of the Ecemiş fault zone from Pinarbasi and south (Fig. 3), the unit has consistent bedding attitudes with ESE to ENE strikes and 30°–45° southerly dips. The stage 2 normal faults record left-lateral, transtensional deformation across the Ecemiş corridor and Niğde Massif; the deformation was accompanied by terrestrial deposition of the Çukurbağ and Burç Formations in isolated subbasins parallel to the Ecemiş fault zone, open folds parallel to the southwesterly regional extension, and major strike-slip faulting on the Ecemiş fault zone that involves the Çukurbağ Formation. The pattern of common Çukurbağ Formation in a belt adjacent to and within the Ecemiş fault zone continues to the south of the study area for ~25 km along the Ecemiş fault zone (Jaffey and Robertson, 2005; Gürer et al., 2016).

The Ecemiş fault zone is mapped as one main fault in the northern part of the corridor but becomes a zone ~1–3 km wide to the south and continues as a few-km-wide zone for ~70 km south of Çamardı to near Gülek (Jaffey and Robertson, 2005). Within and at the boundaries of the Ecemiş fault zone are fault bends that create the subbasins of the Çukurbağ Formation at releasing bends (Figs. 3, 7, and 8) and zones of structural complexity at restraining bends as described below. Ignimbrites with 7–6 Ma ages within and on top of the Cihanbeyli Formation north and south of the Niğde Massif overlie all older units and are not tilted or faulted (Whitney et al., 2008; Radwany et al., 2017; Meijers et al. 2018).

4.1. Celallar Area

The Celallar area (Fig. 4) contains the southern end of the thrust fault that places the eastern belt of the Niğde Massif over the core. The lower calc-silicates and quartzites in the southeast are thrust over the upper massive marbles along a NNE-striking fault (Fig. 4A). On each side of the thrust fault, the foliation in the metasedimentary rocks dips consistently to the SE with a N60° mineral lineation. Near

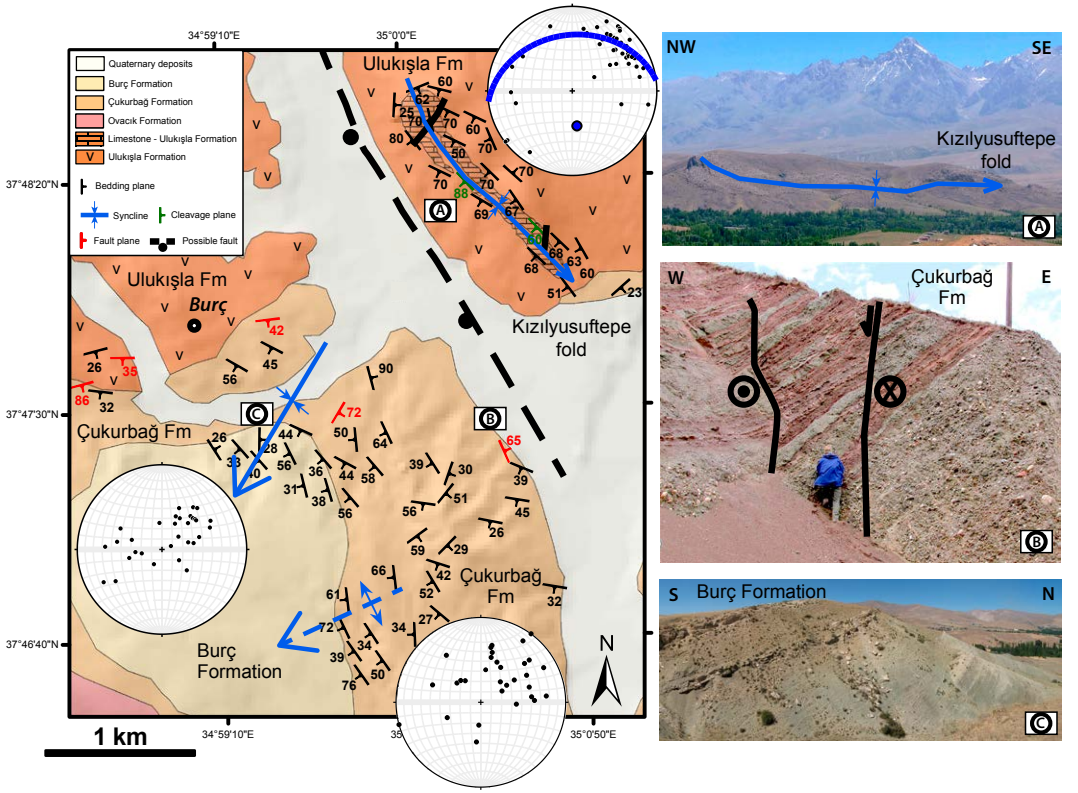

Figure 6. Detailed geologic and tectonic map of the Burç-Kızılyusuftepe area (Burç is village in the west central area), including interpreted field photographs (A–C) and structural data (poles to bedding planes in black dots). The bedding attitudes from the Kızılyusuftepe fold are mainly from the northern part of the fold with the derived girdle and pole (in blue) representative of that area of the fold. The stereonets on the bottom left are bedding from the open syncline with more measurements than are on the map. The stereonets on the bottom right are bedding from the anticline and bedding east of that in the Çukurbağ Formation. Photographs by Côme Lefebvre.

the fault, localized structural features attest to its tectonic nature: (1) coarse-grained foliation of the underlying marble is locally cut by centimeter-scale mylonitic bands showing a drastic grain-size reduction and sheared grain shapes (Fig. 4B). The shear zones strike parallel to the crosscutting foliation with a similar orientation of stretched minerals (red arrows in Fig. 4B). Microscopic field indicators within those deformed bands show asymmetric clasts with a top-to-the-NNE sense of motion. (2) The overlying and rheologically stronger quartzites (Fig. 4C) show intense brittle deformation near the fault, varying from quartzitic breccias to cataclasites.

The overall interpretation of the Celallar area is that it reveals a thrust nappe rooted within the Niğde Massif; the thrust nappe delineates the western border of the Eastern belt of the massif (Fig. 9). Local structures near the fault zone indicate an oblique north-northeastward motion along the thrust contact. The relation of the Paleogene rocks to the Eastern belt thrust nappe is poorly known, but we interpret it to be the southern extension of the thrust fault through the Evliyatepe area, and continuing through Çamardı and SW of Çamardı (Fig. 3). West of the Celallar area, the southern boundary of the Niğde Massif is a SW-down normal fault.

4.2. East-Evliyatepe Area

The East-Evliyatepe area contains parts of three thrust nappes and two thrust faults that strike SSW–NNE across the area and a local mini-graben (~150–200 m E-W by 500 m N-S) of gypsum of the Çukurbağ Formation (Fig. 5). The Ulukışla Formation in the east is thrust over the deep marine sedimentary rocks of the Ovacık Group in the central belt; then, the Ovacık Group is thrust over marginal marine rocks of the Evliyatepe Formation. These marine rocks nonconformably overlie the metamorphic rocks of the Niğde Massif. The Ulukışla Formation over Ovacık Group thrust fault was identified locally in four places from Çamardı north for 8 km (Figs. 3 and 5), and it can be followed nearly continuously on Google Earth imagery. The Ovacık Group over Evliyatepe Formation thrust fault includes a narrow belt (<200 m) of Ulukışla volcanic rocks either deposited below the Ovacık Group (the interpretation on Fig. 5) or faulted between Ovacık Group rocks on the east and Evliyatepe Formation on the west. This belt runs from near

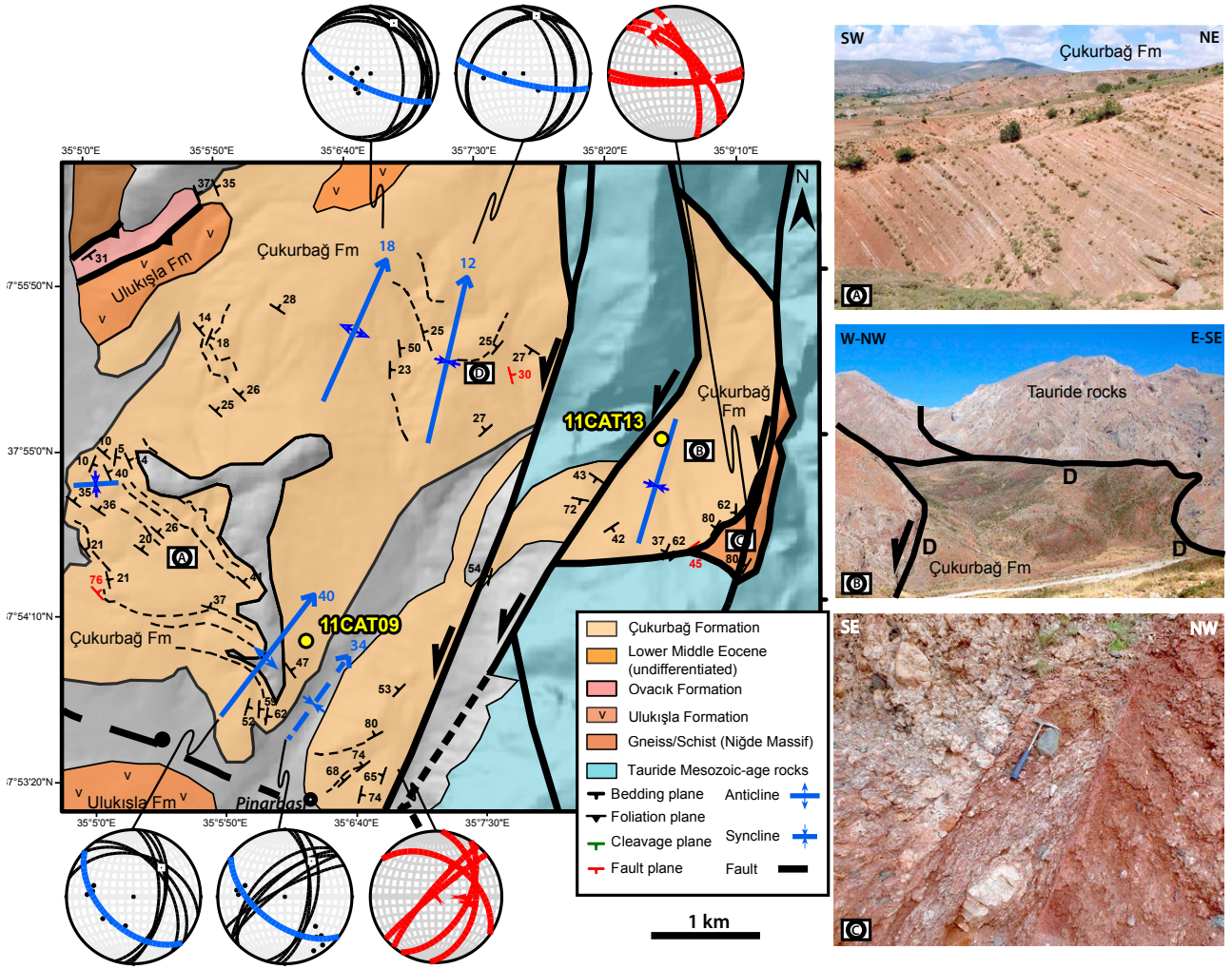

Figure 7. Detailed geologic and tectonic map of the Pinarbaşı area (village on the bottom), including interpreted field photographs (A–C) and structural data (bedding planes and poles in block on stereonet and fault surfaces in red). All stereonet data from near the folds shown except upper-right stereonet with data from location C along the eastern boundary fault of the Ecemiş fault zone. Photographs by Côme Lefebvre.

the mini-graben of Çukurbağ Formation gypsum (C on Fig. 5) south for ~3 km, where the volcanic rocks are cut off by an oblique lateral thrust fault cutting south to join the main Ulukışla thrust fault (Fig. 5) near Çamardı. The Ovacık Group thrust fault continues to the SW through the city of Çamardı and at least 3 km farther to the SW (Fig. 3), where it places Ovacık Group rocks over both the Evliyatepe and Çamardı formations.

Structures in the Ovacık Group are well displayed and exposed in transects along streams, whereas they are generally poorly exposed in the Ulukışla Formation. At one location (Fig. 5A), the Ulukışla thrust fault shows oblique kinematics with a left-lateral component; it has a 028/54/119 strike/dip/rake indicating NNW vergence. In the Ovacık Group, many structural observations support left-oblique thrust faulting, including: (1) three

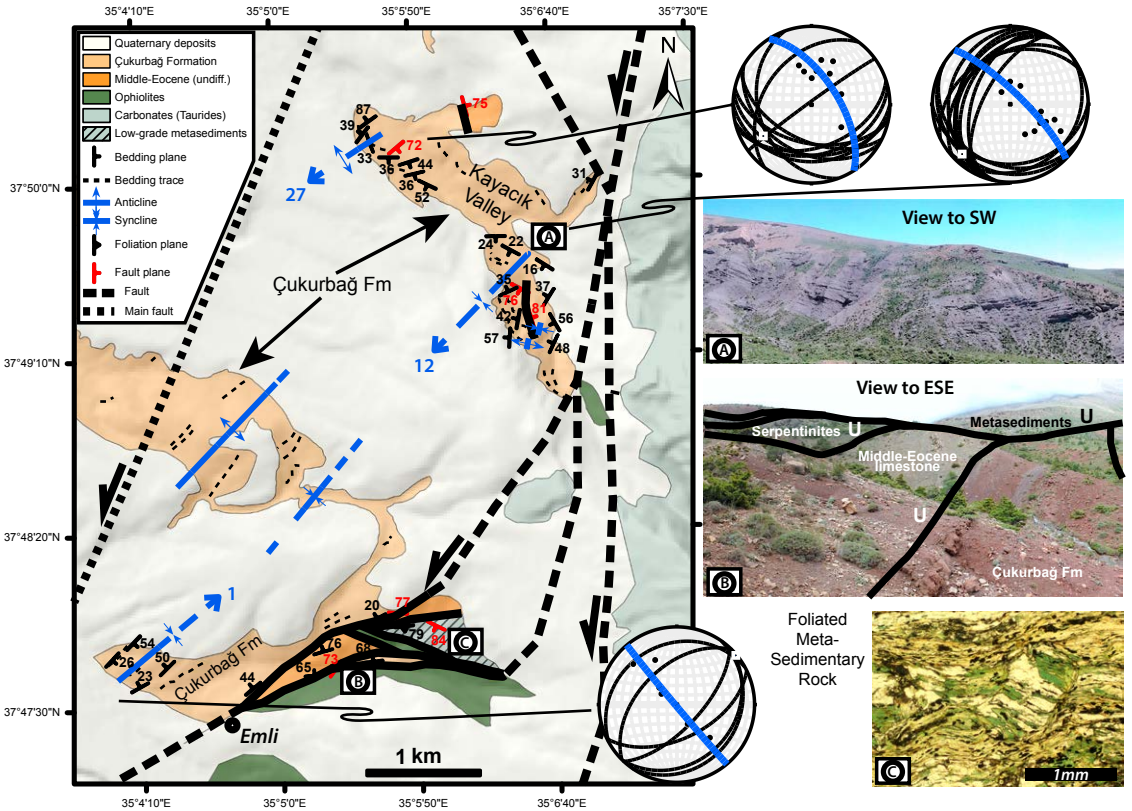

Figure 8. Detailed geologic and tectonic map of the Emli-Kayacık Valley area across the Ecemiş fault zone, including interpreted field photographs (A and B), photomicrograph (C), and structural data (bedding planes and poles are block lines and dots, while fold girdle and pole are in blue). Blue numbers at the head of hinge lines represent the plunge of the folds. Photographs by Côme Lefebvre.

examples of NW-vergent reverse faults (Fig. 5 photograph A) cutting off anticlines that are likely local fault-propagation folds; (2) locally common decimeter- to meter-scale folds with shallow NE to NNE plunges (Fig. 5 photograph B); (3) local asymmetric folds of meter to a few tens of meters scale have mainly SE over NW vergence; and (4) cleavage is locally developed and dominantly NE striking with moderate to steep SE dips.

The mini-graben (Fig. 5C) consists of undated red gypsum and mudstone correlated to the upper Çukurbağ Formation. These rocks are faulted against the Ovacık Group to the east, north, and south. To the west, the Çukurbağ Formation is faulted against the Evliyatepe Formation along a steep fault zone with fault lenses of schist of the Niğde Massif (Fig. 5). The Ovacık Group–Evliyatepe Formation contact is mapped to the south of the mini-graben as an oblique thrust fault.

The overall interpretation of the East-Evliyatepe area is two left-oblique thrust faults with relatively highly deformed Eocene rocks of the Ovacık Group between the two thrust faults (Fig. 9). The Paleocene–Eocene Ulukışla Formation, Ovacık Group, and Evliyatepe Formation were all involved in the deformation; although the Evliyatepe Formation to the west is less deformed in a simple, moderately east-dipping homocline. A later set of normal and oblique-normal faults overprints the older thrust-related structures and forms a mini-graben with red gypsum and mudstone of the Çukurbağ Formation between the Ovacık Group and Evliyatepe Formation.

4.3. Burç-Kızılyusuftepe Area

The Burç-Kızılyusuftepe area lies 2–5 km west of the Ecemiş fault zone (Fig. 3). In the north, the area contains the southern end of the main belt of the Ulukışla Formation in the study area, with a small patch of the Çukurbağ Formation lying across an angular unconformity over the Ulukışla Formation to the south (Fig. 6). A down-to-the-SW normal fault is well defined through the Niğde Massif to the NW and is interpreted to continue along the river valley between the NE block and the southwestern part of the Burç subbasin (Figs. 3 and 6). The Ulukışla Formation to the northwest near the village of Burç is overlain to the south across an angular unconformity by the Çukurbağ Formation, which in

turn is overlain conformably by the Burç Formation (Fig. 6C). The Çukurbağ-Burç succession forms a km-scale, SW-plunging open syncline. To the southeast, the upper Çukurbağ and lower Burç is a very open anticline, while the middle Çukurbağ strata are more complexly deformed, and the lower (eastern) Çukurbağ beds dip moderately south (Fig. 6). On the highway SE of Çamardı (east side of the Fig. 6 map), good outcrops of Çukurbağ Formation sandstone and conglomerate with map-scale folds have common NNW-striking, oblique left-normal faults spaced a few meters to tens of meters apart (Fig. 6B). Closer to the Ecemiş fault zone, similar facies of the Çukurbağ Formation ~500–600 m from the main fault near the village of Elekgölü have steep, mainly N-S–striking bedding in a syncline subparallel to the Ecemiş fault zone (Fig. 3).

The Kızılyusuftepe limestone (NE part of Fig. 6 map and photograph A) demonstrates that the Ulukışla Formation is locally highly deformed. The Kızılyusuftepe fold in limestones is surrounded by volcanic rocks of the Ulukışla Formation. The fold is almost 2 km long and is an overturned syncline steeply plunging to the SE with the SW limb overturned (Fig. 6A and stereonet). The red sandstone and shale in the fold interior have local cleavage and small folds. The fold is cut by two NW-striking, right-lateral oblique normal faults with ~150 and 100 m of separation of the northeast limb of the syncline, but not well resolved at the scale of Figure 6. The overturned SW limb is highly thinned by faulting. We observed at least three other places in the study area not illustrated here where similar relations occurred in limestones of the Ulukışla Formation with tight folds cut by either N- to NE-striking, left-lateral faults or NW-striking, right-lateral faults.

The overall structural interpretation of the south-central part of the Ecemiş corridor near Burç is that the Ulukışla Formation is locally strongly deformed into tight to isoclinal overturned folds, and later broadly folded and cut by dominantly N-S to NNW left-lateral faults and NW-striking, right-lateral oblique faults. The Burç and Çukurbağ formations lie across angular unconformities above the Ulukışla Formation and are deformed into open to moderately tight folds that show progressively more deformation toward the Ecemiş fault zone. The Burç and Çukurbağ formations are also faulted by NW-striking normal faults.

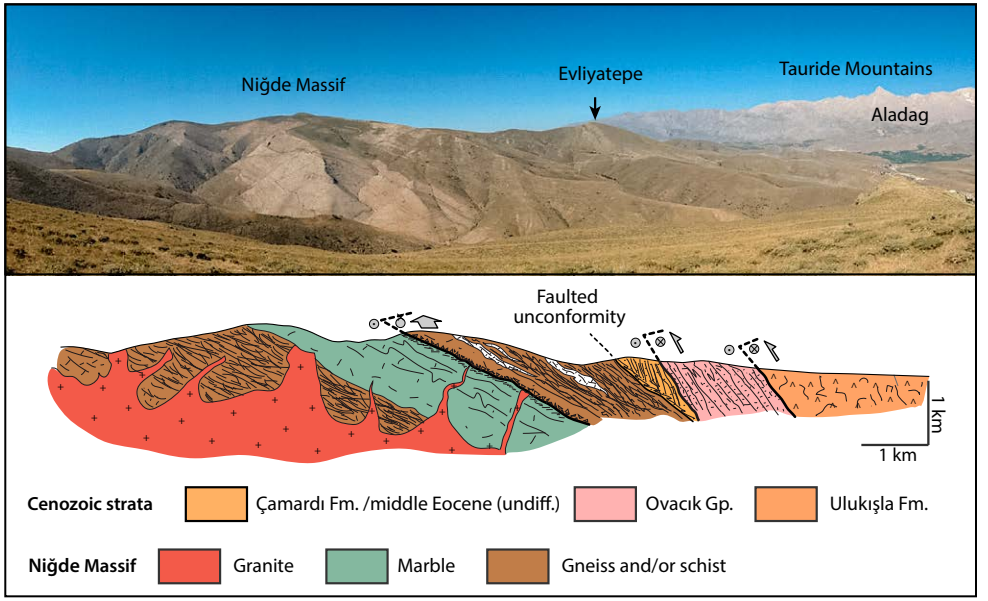

Figure 9. Photograph and cross section across the Ecemiş corridor and eastern Niğde Massif showing the relation of the main oblique thrust faults. View is to the northeast; location of section on Figure 3. The Ecemiş fault zone runs along the base of the Tauride Mountains (Aladağ) on the far right side of the photograph. Photograph by Côme Lefebvre.

4.4. Pinarbaşı Area

The Pinarbaşı area consists of a 2-km-wide Ecemiş fault zone on the east and a 3–4-km-wide belt of Çukurbağ Formation in the main Ecemiş corridor (Fig. 7). The Çukurbağ Formation is deposited on the Ulukışla Formation in the northwest, which in turn is interpreted to be thrust over the Ovacık Group and that unit thrust against the metamorphic rocks of the Niğde Massif to the NNW.

The Ecemiş fault zone here consists of major faults on the eastern and western edges of the zone. The western fault consists of lenses of Mesozoic limestones and steeply bedded Çukurbağ Formation and minor Eocene rocks in a 100–150-m-wide fault zone. A major fault in the middle of the Ecemiş fault zone runs N-S and then takes a bend to the southwest and joins the western fault. A bend to the SE from the same fault to the eastern boundary fault is a releasing step and may explain the mini-basin or down-dropped block of Eocene Ovacık Group and Çukurbağ Formation sedimentary rocks (Fig. 7, photograph B). The southern part of the mini-basin was studied in detail and shows a moderately open, NNE-plunging syncline in the Ovacık Group rocks with a steeper eastern limb and local folds that also have a NNE plunge (too small to show on Fig. 7). A local 0.5-m-wide, steeply dipping fault zone in the Ovacık Group shows SE over NW dip-slip kinematics of R shears and rotated clasts (Fig. 7, photograph C). Common secondary faults in that zone are NW striking with shallow striae of right-lateral and unknown slip directions (Fig. 7C and stereonet). The Çukurbağ Formation is highly faulted on the east against the Ovacık Group

rocks. A 40-m-wide fault strand cuts through the Çukurbağ Formation with cm-scale fault fabric that strikes 195°–205° and dips west 70°–55°.

The Çukurbağ Formation west of the Ecemiş fault zone forms the main Bademdere subbasin that generally dips to the NNE and forms a series of NNE-plunging open folds; the syncline-anticline pair in the south may gently curve to be the same folds as the similar pair to the north (Fig. 7 map and stereonets). Bedding dips are generally moderate (20°–50°) with gentler dips on the west and steep dips and strikes that parallel the Ecemiş fault zone on the east (Fig. 7). On the east limb of the northern syncline (Fig. 7D) are three few-m-scale, down-to-the-NE normal faults formed during Çukurbağ Formation deposition as they are directly overlain by unfaulted beds.

Most of the strata of the Çukurbağ Formation in the Bademdere subbasin are notably less deformed than the Eocene units within the Ecemiş corridor to the south. There are many fewer secondary faults and folds and no cleavage. In contrast, the Çukurbağ Formation is steeply bedded and has scattered to locally abundant small faults for the few hundreds of meters near the Ecemiş fault zone, and it shows moderate to locally intense deformation along the western and eastern boundary faults of the Ecemiş fault zone as described above.

A 1200-m-long traverse through a well-exposed strand of the Ecemiş fault zone along an irrigation canal 600 m NE of Demirkazık ("D" in Fig. 3) is between the Pinarbaşı and Emli local areas (Figs. 7 and 8). On the east are Eocene sedimentary rocks (Ovacık Group) (too small to show on Fig. 3) with common (few decimeter spacing) small faults and fractures and cataclastic cleavage (240°/50°). Thirteen small faults in this moderately deformed zone are mainly 45°–70°–striking, right-lateral faults and 180°–210°–striking, left-lateral faults with steep dips (~60°–89°) compatible with overall left-lateral, strike-slip faulting. A 5-m-wide fault zone at the contact of the Ovacık Group and Çukurbağ Formation has subvertical fault fabrics and moderately plunging small folds. A secondary fault next to and parallel to the fault zone has a 204°/89°/175° (strike/dip/rake) orientation with left-lateral, strike-slip kinematics. In the few tens of meters west of the fault zone, the Çukurbağ Formation has common veins and similar secondary faults as the Eocene rocks to the east, but with cm and then decimeter spacing.

4.5. Emli-Kayacık Valley Area

The Emli-Kayacık Valley area is entirely within the Ecemiş fault zone (Fig. 3) and forms a 4–8-km-long area of mainly Çukurbağ Formation with local fault lenses of probable Ovacık Group (middle Eocene undifferentiated on Fig. 8). The area is bounded on the north by a likely NW-striking fault placing the Ecemiş corridor Cenozoic rocks against Mesozoic limestones and on the south by mainly ophiolitic rocks of the Taurides (Fig. 8). In essence, this is another local mini-basin or down-dropped block within the Ecemiş fault zone, similar to the mini-basin in the Pinarbaşı area, though the Emli area may be a more classic pull-apart basin. The faults on the south to southeast merge to the north to become the eastern boundary of the Ecemiş fault zone (eastern faults on Fig. 8); the same faults cut across to the western boundary fault to the southwest (Fig. 3). The extensive Çukurbağ Formation exposures within the Ecemiş fault zone in this area define a series of moderately open folds with NE-SW trends (Fig. 8 map, stereonets, and photograph A), oblique to the strike of the Ecemiş fault zone. The folds plunge to the SW in the north and to the NE in the south or toward the center of the Emli-Kayacık Valley mini-basin.

Deformation within the Ecemiş fault zone is much higher strain on the SE and southern sides than in the rest of the Emli-Kayacık Valley area. In the Kayacık Valley in the north (Fig. 8), the southeastern limit of exposed Çukurbağ Formation is marked by a NNW-striking, left-lateral fault with abundant veins and an apparent west-over-east component of faulting. Local open folds have asymmetry compatible with the left-lateral Ecemiş fault zone, while an anticline next to the fault is tighter than the larger open folds to the west (Fig. 8A). At the SE and upper end of Kayacık Valley, the Çukurbağ Formation is faulted against Mesozoic ophiolitic rocks (Fig. 8). To the south, 2–3 km, near the small village of Emli, is a complex fault wedge consisting of steeply bedded ENE- to E-W–striking, north-dipping Eocene rocks (Ovacık Group) and foliated Mesozoic ophiolitic and metasedimentary rocks faulted against each other (Fig. 8, photographs B and C); most local fault relations suggest a component of thrust faulting. The shape and orientation of the faulted units in the fault wedge strongly suggest complex oblique faulting and not an orderly set of thrust faults. Scattered small faults are also mainly E-W striking. The wedge is fault-bounded to the south against a narrow slice of Çukurbağ Formation and larger area of Tauride ophiolitic rocks. To the north, the wedge is faulted against the broadly folded belt of Çukurbağ Formation (Fig. 8). The metasedimentary rocks in the eastern part of the fault wedge are important because no ophiolitic and metasedimentary rocks are known in the adjacent Taurides until outcrops of Yahyalı metamorphic rocks ~30–40 km to the north on the east side of the Ecemiş fault zone (Fig. 2) (Dirik et al., 1999; Pourteau et al., 2010).

The overall interpretation of this area is that the Çukurbağ Formation was deposited within a local pull-apart basin within the Ecemiş fault zone, and was then deformed by continued strike-slip faulting after deposition. The southern fault wedge of more highly deformed and older rocks lies along a restraining bend in the larger left-lateral Ecemiş fault zone.

5. GEOCHRONOLOGY AND THERMOCHRONOLOGY

Samples from the Ecemiş corridor were collected from the Paleocene–Eocene Ulukışla Formation and Oligo-Miocene Çukurbağ Formation for geochronology and thermochronology to constrain the depositional age and provenance of the units and to date their burial and later exhumation. $^{40}Ar/^{39}Ar$ dating of volcanic rocks was used to date depositional age, and detrital zircon (DZ) U-Pb dating was conducted to determine the maximum depositional age of sedimentary rocks. Apatite and zircon fission-track (AFT and ZFT) and apatite helium (AHe) cooling ages were obtained to date exhumation, and where they were not reset, to

determine provenance. In this section, we report the results (see Supplemental Material[1]) and then narrowly interpret those results. In the Discussion, we put the interpretations of the geochronology and thermochronology in the broader context of the history of the study area.

5.1. $^{40}Ar/^{39}Ar$ Dating

We obtained a $^{40}Ar/^{39}Ar$ plateau age of 58.8 ± 0.8 Ma (57.3 ± 1.2 Ma total gas age) on biotite from an andesite (sample 17613a) within a map-scale overturned syncline (Kızılyusuftepe fold), 3 km east of Burç (Figs. 3 and 10). This location is interpreted to be relatively high in the Ulukışla Formation. The U-Pb zircon ages of 59.6 and 59.7 Ma from the Ulukışla Formation in the main basin to the south (Gürer et al., 2016) and $^{40}Ar/^{39}Ar$ biotite age of 58.8 Ma in this study taken together suggest that the age of the Ulukışla Formation is ca. 60 Ma in the northern Ulukışla basin and Ecemiş corridor.

Two nearby samples of basalt yielded whole-rock $^{40}Ar/^{39}Ar$ total gas ages of 37 ± 3 Ma (11TR01 0.5 km SW of Burç) and 41.99 ± 0.18 Ma (21613a on the NE side of the Kızılyusuftepe fold). In addition, sample 21613a yielded a weighted-mean plagioclase age of 39.6 ± 1.5 Ma. One of these younger samples (21613a) is mapped 100–200 m stratigraphically below the 17613a sample with a much older $^{40}Ar/^{39}Ar$ age, in apparent conflict with their stratigraphic position. However, these younger ages are from the Ulukışla Formation thrust nappe (Fig. 3) and may have experienced partial argon loss during thrusting, consistent with the range of plagioclase ages in sample 21613a.

5.2. Detrital Zircon U-Pb Dating

The Çukurbağ Formation comprises largely non-fossiliferous fluvial sediments, making its depositional age, and hence the maximum age span of the regional late Eocene to early Miocene unconformity, poorly constrained. To constrain the maximum depositional age of the Çukurbağ Formation, we applied large-n detrital zircon (DZ) U-Pb dating (see Supplemental Material for methods [footnote 1]) to three Çukurbağ Formation samples in the Ecemiş corridor: 11CAT03 from its western part immediately south of the Niğde Massif (Fig. 3); and two samples from the Pinarbaşı area (Fig. 7): 11CAT09, from folded rocks ~2 km west of the main Ecemiş fault zone; and 11CAT13 from the small mini-basin within of the main Ecemiş fault zone (Figs. 3 and 7B). The results of these analyses are shown in Figure 11.

5.2.1. Maximum Depositional Ages

In two of the three samples, we obtained a small fraction of Oligo-Miocene zircon grains to provide meaningful maximum depositional ages (MDAs). In sample 11CAT09, a youngest DZ age peak of 21.9 ± 0.6 Ma is defined by five DZ ages (from a total of 298 grains analyzed). In sample 11CAT13, a youngest age peak of 24.9 ± 0.4 Ma is defined by seven DZ ages (from a total of 356 grains analyzed). These data support a maximum early Miocene (or very latest Oligocene for sample 11CAT13) MDA for the Çukurbağ Formation in the Ecemiş corridor. The source of these younger grains is uncertain, since no felsic magmatism or volcanism of this age is known from central Anatolia (Schleiffarth et al., 2018). Instead, we suspect, given the very low abundance of these younger grains and their euhedral volcanic crystal form, that they represent air-fall grains derived from voluminous Oligocene and early Miocene volcanism and magmatism in northwest Turkey and the northern Aegean (e.g., Dilek and Altunkaynak, 2009; Ersoy and Palmer, 2013).

5.2.2. Detrital Zircon Provenance Constraints

The DZ ages from all three samples also provide important information on the provenance of the Çukurbağ Formation subbasins of the Ecemiş corridor. Sample 11CAT03 (Figs. 11A and 11D), while containing no Oligo-Miocene zircon grains, does contain four distinct age peaks that support a local source for these rocks. The 49.6 ± 0.2 Ma and 56.3 ± 0.2 Ma peaks match ages of the 49–51 Ma Horoz granite (Parlak et al., 2013; Gürer et al., 2018) intruded into high-pressure metamorphic rocks of the Anatolide-Tauride Block (Tauride Mountains, Fig. 2) immediately to the south of the Ulukışla basin, and the 56.1–56.2 Ma (Gürer et al., 2018) Elmalı syenite intruded into Paleocene sedimentary rocks of the Ulukışla basin ~30 km to the southwest of sample 11CAT03. The two Cretaceous DZ age peaks (74.6 ± 0.3 Ma and 86.6 ± 0.3 Ma) match well with two main phases of granitoid magmatism dated in the western CACC (Fig. 2) of 82–84 Ma and 74 Ma (Köksal et al., 2011). The older peak also matches well with the 78–89 Ma zircon U-Pb age peak from the Üçkapılı granite in the Niğde Massif immediately to the north of sample 11CAT03 (Fig. 3) (Whitney et al. 2003). The source for the few older DZ ages in 11CAT03 is uncertain, but older pre-Cretaceous zircon U-Pb ages were obtained by Whitney et al. (2003) from a sillimanite schist of the Niğde complex and in zircon cores from the Üçkapılı granite. In summary, the DZ data support a SW-to-NW source for Çukurbağ Formation sample 11CAT03 in the western part of the Ecemiş corridor.

Sample 11CAT09 shows a similar DZ age distribution to sample 11CAT03 (Figs. 11B and 11D), dominated by essentially the same four DZ age peaks at 49.1 ± 0.3 Ma, 55.9 ± 0.3Ma, 75.7 ± 0.4 Ma, and 86.5 ± 0.3 Ma, implying a similar source from the Taurides and Ulukışla basin to the southwest and the CACC to the northwest. The only difference is that sample 11CAT09 contains an additional population of older, pre-Cretaceous DZ grain ages. One possible source of grains older than ca. 500 Ma is sillimanite schist of the Niğde Massif from which such inherited zircon U-Pb ages were reported by Whitney et al. (2003). However, given the significant number of older DZ grain ages younger than ca. 500 Ma not recorded in the sillimanite schist, possible alternative sources for these zircon grains are metamorphosed Paleozoic–Triassic phyllites, quartzites, and Permo-Triassic volcaniclastic rocks within the Bünyan metamorphic rocks within the northernmost part of the eastern Taurides, which now form the basement to the southwestern part of the Sivas Basin (Fig. 2) (Dirik et al., 1999; Pourteau et al., 2010). These results would imply that sample

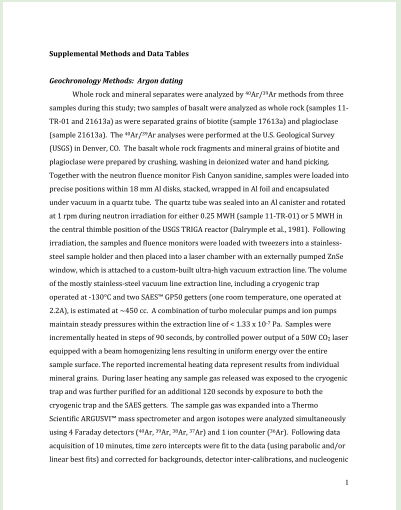

Supplemental Methods and Data Tables

Geochronology Methods: Argon dating

Whole rock and mineral separates were analyzed by $^{40}Ar/^{39}Ar$ methods from three samples during this study; two samples of basalt were analyzed as whole rock (samples 11-TR-01 and 21613a) as were separated grains of biotite (sample 17613a) and plagioclase (sample 21613a). The $^{40}Ar/^{39}Ar$ analyses were performed at the U.S. Geological Survey (USGS) in Denver, CO. The basalt whole rock fragments and mineral grains of biotite and plagioclase were prepared by crushing, washing in deionized water and hand picking. Together with the neutron fluence monitor Fish Canyon sanidine, samples were loaded into precise positions within 18 mm Al disks, stacked, wrapped in Al foil and encapsulated under vacuum in a quartz tube. The quartz tube was sealed into an Al canister and rotated at 1 rpm during neutron irradiation for either 0.25 MWH (sample 11-TR-01) or 5 MWH in the central thimble position of the USGS TRIGA reactor (Dalrymple et al., 1981). Following irradiation, the samples and fluence monitors were loaded with tweezers into a stainless-steel sample holder and then placed into a laser chamber with an externally pumped ZnSe window, which is attached to a custom-built ultra-high vacuum extraction line. The volume of the mostly stainless-steel vacuum line extraction line, including a cryogenic trap operated at -130°C and two SAES™ GP50 getters (one room temperature, one operated at 2.2A), is estimated at ~450 cc. A combination of turbo molecular pumps and ion pumps maintain steady pressures within the extraction line of < 1.33×10^{-7} Pa. Samples were incrementally heated in steps of 90 seconds, by controlled power output of a 50W CO_2 laser equipped with a beam homogenizing lens resulting in uniform energy over the entire sample surface. The reported incremental heating data represent results from individual mineral grains. During laser heating any sample gas released was exposed to the cryogenic trap and was further purified for an additional 120 seconds by exposure to both the cryogenic trap and the SAES getters. The sample gas was expanded into a Thermo Scientific ARGUSVI™ mass spectrometer and argon isotopes were analyzed simultaneously using 4 Faraday detectors (^{40}Ar, ^{39}Ar, ^{37}Ar) and 1 ion counter (^{36}Ar). Following data acquisition of 10 minutes, time zero intercepts were fit to the data (using parabolic and/or linear best fits) and corrected for backgrounds, detector inter-calibrations, and nucleogenic

1

[1]Supplemental Material. Consists of geochronology and thermochronology data, and methods related to those data. Geochronology data are from $^{40}Ar/^{39}Ar$ dating of volcanic rocks and U-Pb analysis of detrital zircons, while thermochronology data are from apatite and zircon fission-track and apatite helium cooling ages. Please visit https://doi.org/10.1130/GEOS.S.12971792 to access the supplemental material, and contact editing@geosociety.org with any questions.

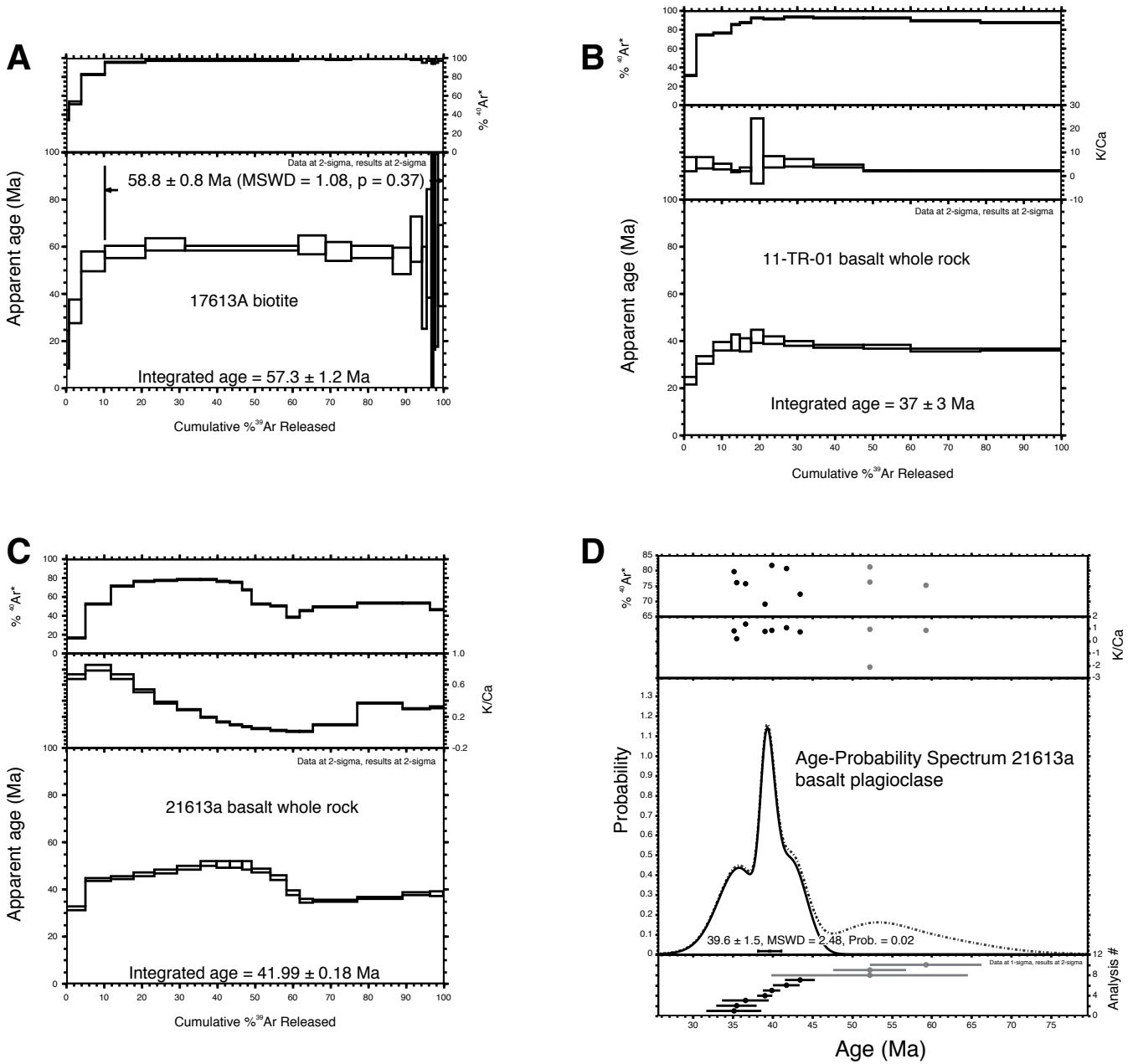

Figure 10. $^{40}Ar/^{39}Ar$ spectra from volcanic rocks of the Ulukışla Formation. Sample location for sample 17613A shown in Figure 3. (A) Biotite spectra sample 17613A. (B) Whole-rock spectra from sample11TR01. (C) Whole-rock spectra from sample 21613A. (D) Plagioclase spectra from sample 21613A. See text for discussion of the results.

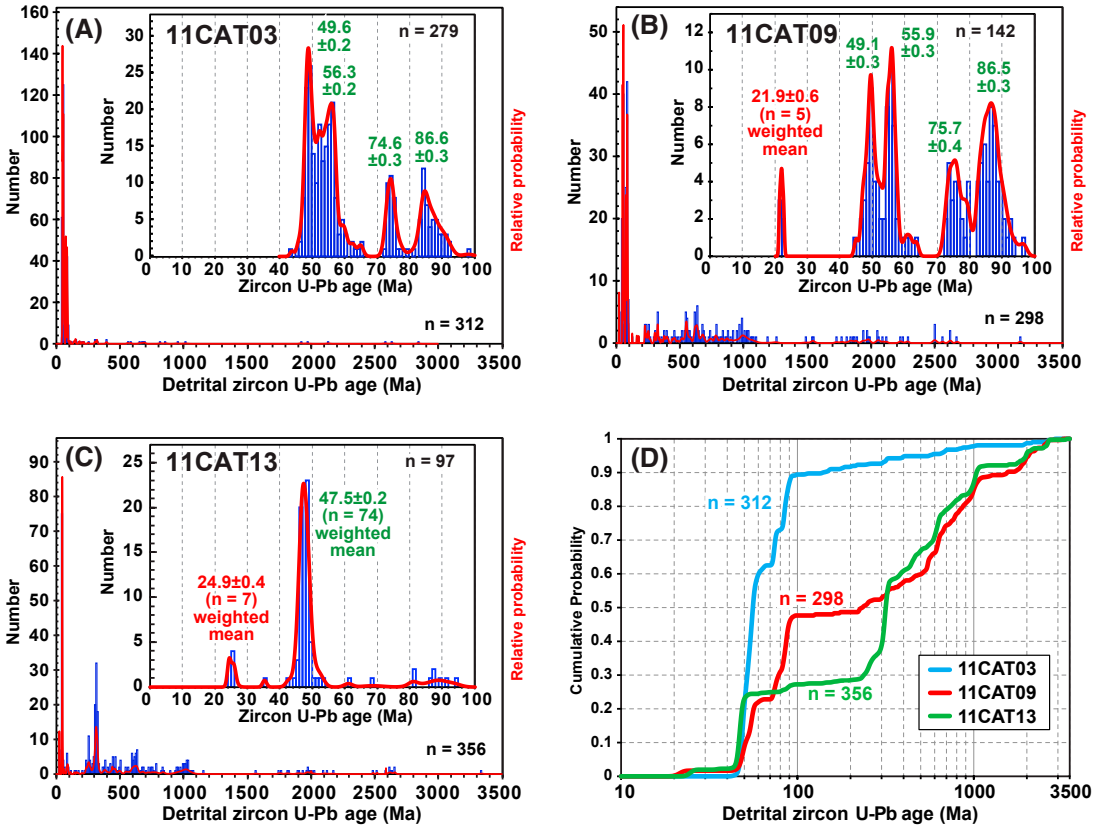

Figure 11. Detrital zircon U-Pb results shown as age histograms and probability density plots in (A) to (C) with insets showing ages younger than 100 Ma. In red are weighted-mean ages of the youngest age population used to constrain maximum depositional age in these two samples. Approximate ages of other major age peaks are also shown. (D) The same data plotted in the form of cumulative probability that highlights the differences in detrital zircon provenance between each of the samples.

11CAT09 has a mixed sediment source from both east and west of the Ecemiş corridor.

Çukurbağ Formation sample 11CAT13 shows a very distinct DZ age signature (Figs. 11C and 11D). This sample is dominated by a single 47.5 ± 0.2 Ma peak that matches the 47–49 Ma Karamadazı or Yahyalı granitoid (Kusçu et al., 2010) ~30 km to the NNE. We rule out a source related to the similarly aged Horoz granitoid to the southwest because, in this case, we would also expect a 56 Ma DZ age peak from the Elmalı syenite within the Ulukışla basin located in the same general southwesterly catchment direction. The almost complete lack of ca. 75–90 Ma CACC-derived zircon grains rules out a more westerly source for sample 11CAT13, implying either a very localized source solely to the NNE, or, because it lies within the main Ecemiş fault zone, this sample may have moved tens of km to its current position relative to rocks west of the fault zone by Miocene and younger left-lateral translation. This sample also contains a significant ca. 240–330 Ma DZ age peak and older zircon grains likely sourced from the Bünyan metamorphic unit (Fig. 2), in the same general region as the Karamadazı granitoid. Similar metamorphic rocks are also seen in the small fault wedge in the Emli-Kayacık Valley area (section 4.5, Figs. 2 and 8), ~5 km to the south of sample 11CAT13. These results further support a northeasterly source for the fluvial sediments within this mini-basin.

The presence of this distinct Variscan-age DZ peak from rocks of the Anatolide-Tauride block is unusual. The Anatolide-Tauride block is characterized by basement rocks of Cambrian (Pan-African) age with Gondwanan affinity south of the former Paleotethys Ocean. Most Variscan-age magmatism and tectonism in Anatolia are restricted to the basement of the Pontides on the former southern margin of Laurasia, north of the İzmir-Ankara suture zone (Candan et al., 2016). However, local Carboniferous metagranites have recently been described from the Afyon zone on the northern margin of the Anatolide-Tauride block in westernmost Turkey and are also known from northwestern Iran (Candan et al., 2016); these metagranites may have acted

as a source for detrital zircon of this age within the Bünyan Permian–Triassic metasedimentary rocks that were subsequently recycled into the Miocene Çukurbağ Formation rocks of samples 11CAT09 and 11CAT13.

5.3. Detrital Zircon Fission-Track Dating

Detrital zircon fission-track (dZFT) dating results from 16 sedimentary rock samples in the Ecemiş corridor (Fig. 3) are shown as probability density plots and histograms in Figure 12, with plots arranged in a schematic map format. The first important observation is that none of the samples show reset dZFT grain ages younger than the estimated stratigraphic age of these rocks. Partial resetting of ZFT ages in radiation-damaged detrital zircon is considered not to occur until temperatures reach at least 175 °C for a heating time of 25 m.y. (Reiners and Brandon, 2006). Thus, none of the sampled rocks have been buried to depths of >~6.5 km (assuming a conservative geothermal gradient of 25 °C/km and annual mean surface temperature of 10 °C) following deposition. These <6.5 km burial depths are expected given the maximum stratigraphic thickness of the Çukurbağ Formation above the late Eocene to late Oligocene basin-wide unconformity but provides an important limit for maximum deposition (and structural) burial of the Paleogene rocks below the unconformity, as well as providing an upper limit on the amount of missing section represented by the unconformity.

Zircon yield was very low in many of these samples (most of these sedimentary rocks derive from a zircon-poor ophiolitic and carbonate source; Radwany et al., 2017), and therefore very few dZFT single-grain ages were found similar to the expected depositional age, and such constraints were imprecise. Nevertheless, two samples from the Çamardı Formation (11CAT04 and 11CAT12) do show dZFT age peaks of 48 ± 3 Ma and 54 ± 3 Ma, respectively (Fig. 12), consistent with previous early to mid-Eocene stratigraphic ages assigned to these rocks (see section 3). Likely sources for such syndepositional age zircon are the ca. 56 Ma Elmalı and ca. 50 Ma Horoz felsic intrusions a few tens of km to the south of these samples (Gürer et al., 2018). Alternatively, the younger dZFT ages from these two samples may reflect partial resetting of the ZFT system, since K-feldspar $^{40}Ar/^{39}Ar$ ages from basement rocks of the Niğde Massif immediately underlying the nonconformity indicate latest Eocene to Oligocene (35 ± 5 Ma) reheating of these rocks to temperatures of 200–300 °C (section 5.1 above; Idleman et al., 2014). The dZFT results from other samples did not provide any anticipated new constraints on depositional age; although they do provide useful new information on the provenance of the various sedimentary units of the Ecemiş corridor.

Detrital zircon grains from the other pre-unconformity (Eocene and older) rocks of the Evliatepe and Ulukışla Formations, and Ovacık Group in the western part of the study, show broad dZFT Late Cretaceous age peaks between 66 Ma and 75 Ma (Fig. 12). Such ages match well with Late Cretaceous granitoid crystallization ages and $^{40}Ar/^{39}Ar$ cooling ages in the CACC (ca. 72–89 Ma, Whitney et al., 2003; Gautier et al., 2008; Köksal et al., 2011; Idleman et al., 2014), suggesting a local provenance, and confirm that basement rocks of the Niğde Massif were exposed at the surface during the Paleocene–Eocene (Umhoefer et al., 2007; Gautier et al., 2008). The dZFT results from the postunconformity Çukurbağ Formation largely mirror the patterns seen in our DZ U-Pb results (section 5.2) in showing a marked contrast in dZFT age signatures west of versus within the Ecemiş fault zone. The four dated samples within the Ecemiş fault zone show almost no 60–90 Ma dZFT grain ages, thus ruling out a westerly CACC-derived source. Instead, two samples (11CAT13 and 11CAT14) show age peaks at ca. 42–48 Ma. We presume these age peaks reflect zircon sourced from the 47–49 Ma Karamadazı or Yahyalı granitoid to the NNE, as also seen in the DZ U-Pb data for sample 11CAT13. All four of these samples also show a distinct population of Mesozoic dZFT grain ages absent in all but sample 11CAT09 west of the Ecemiş fault zone. We postulate these older dZFT-age grains reflect the same source as similar older DZ U-Pb–age zircon seen in sample 11CAT13, including Paleozoic–Triassic phyllites, quartzites, and Permo-Triassic volcaniclastic rocks of the Bünyan metamorphic unit exposed within the Taurides to the northeast (Fig. 2). The dZFT age pattern in the Çukurbağ Formation samples west of the Ecemiş fault zone is dominated by local CACC-sourced 60–80 Ma dZFT grain ages, and younger 46–55 Ma dZFT ages of similar age to Horoz and Elmalı intrusions a short distance to the south. The only exception is sample 11CAT09, which shows an additional group of Mesozoic-age dZFT grain ages seen in samples to the east on the Ecemiş fault zone, supporting a mixed provenance from both the east and west of the Ecemiş corridor as also inferred from the DZ U-Pb grain ages from this same sample.

5.4. Apatite Fission-Track and (U-Th)/He Dating

Our new apatite fission-track (AFT) and (U-Th)/He (AHe) results from the Ecemiş corridor sedimentary rocks are shown in Figure 13 with the AFT probability density plots and histograms arranged schematically in relation to the Ecemiş fault zone and the major late Eocene to early Miocene unconformity. Four Çamardı and Evliatepe Formation samples closest to the Niğde Massif (11CAT04, 06, 07, and 12) all show early Miocene reset AFT ages of ca. 19–20 Ma and AHe grain ages of 13–20 Ma. Reset AFT ages imply these rocks were buried to temperatures >~120 °C following deposition (the temperature required to fully anneal apatite fission tracks of average composition for heating time of 25 m.y.; Reiners and Brandon, 2006) equivalent to depths >~4 km for an average geothermal gradient of 25 °C/km. Similar AFT and AHe ages, along with long mean apatite confined fission-track lengths of ~14.3 µm from three of these samples (Supplemental Material, Table S1 [footnote 1]), imply rapid early Miocene cooling of these rocks following maximum burial. All four of these samples are from just above the nonconformity with basement of the Niğde Massif within the western thrust nappe above our newly identified western thrust fault that displaces the eastern belt of the Niğde Massif over the core of the massif (Fig. 4) but in the footwall to the major overthrust of Ovacık Group rocks to the east (Fig. 5). Thus at least part (most?) of the >4 km postdepositional burial may have been a result of structural, rather than sedimentary, burial.

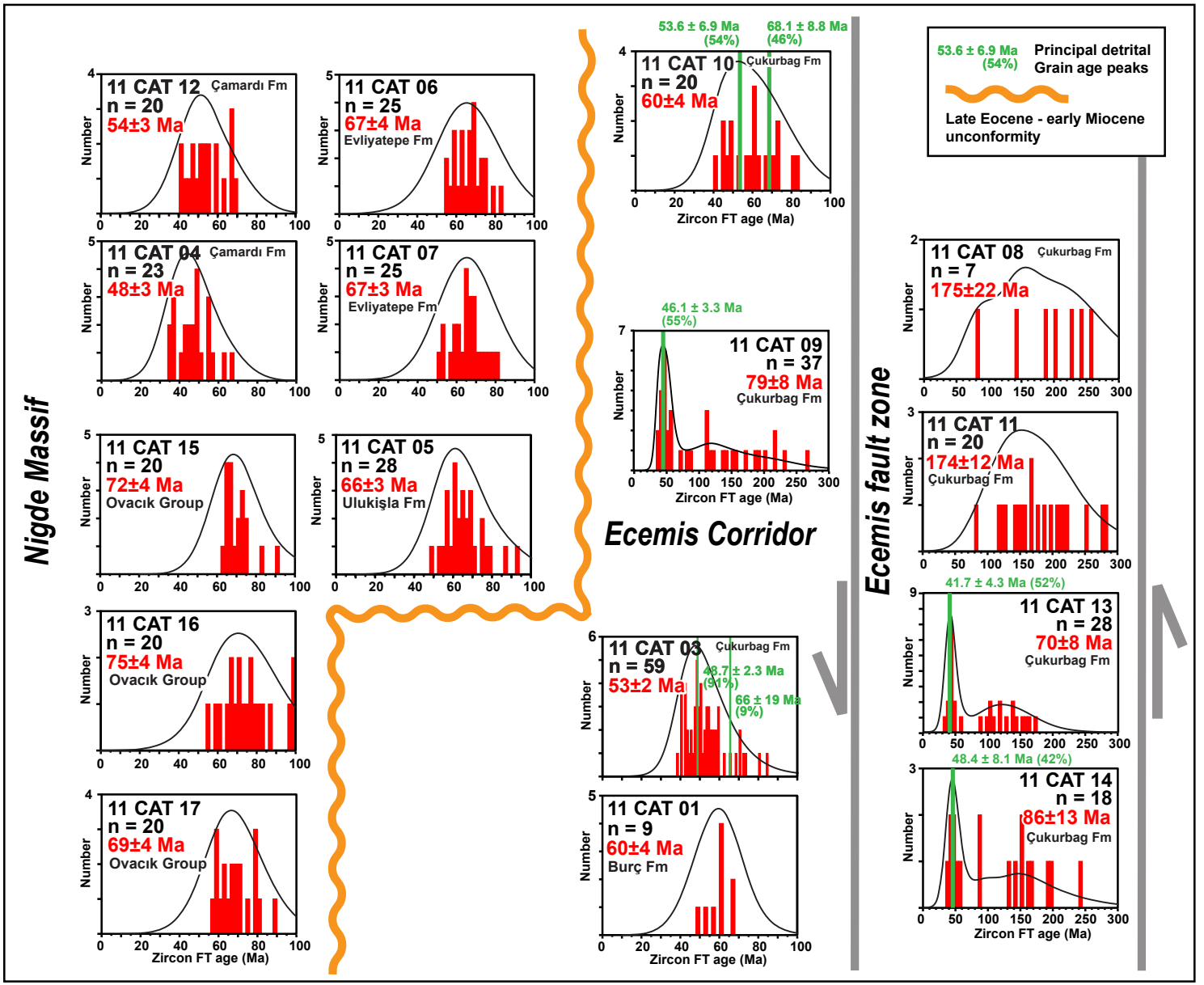

Figure 12. Detrital zircon fission-track (FT) results from the sedimentary rocks of the Ecemiş corridor shown as age histograms and probability density plots. Locations of samples are shown in Figure 3. Here the samples are shown in schematic location form in relation to the Niğde Massif, the late Eocene–early Oligocene unconformity, and the Ecemiş fault zone. Principal detrital grain age components for sample 11CAT01 were calculated using IsoplotR (Vermeesch, 2018).

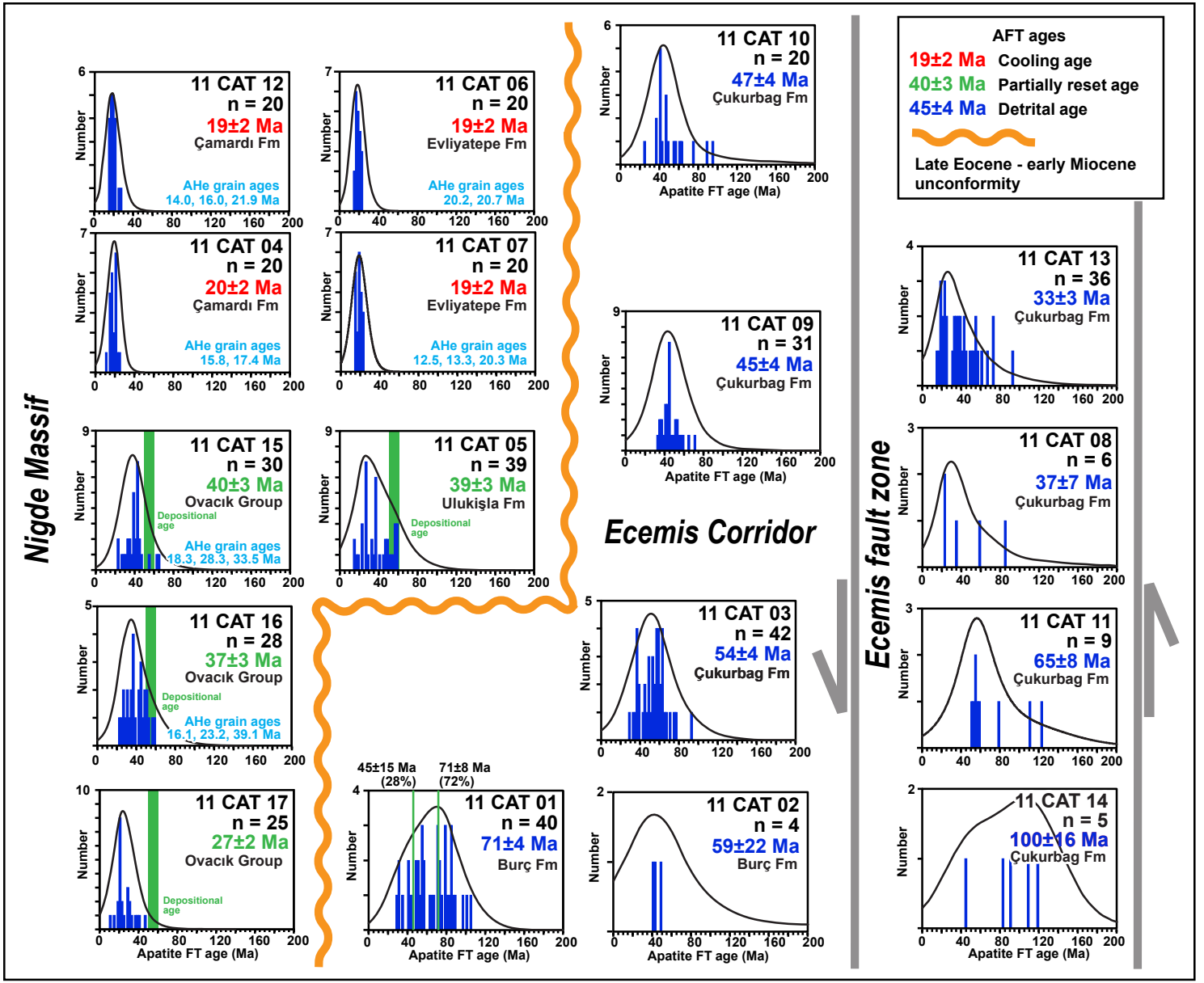

Figure 13. Apatite fission-track (AFT) results from the sedimentary rocks of the Ecemiş corridor shown as age histograms and probability density plots. Single-grain apatite (U-Th)/He ages are shown in light blue text. Locations of samples are shown in Figure 3. Here the samples are shown in schematic location form, as in Figure 12. Principal detrital grain age components shown in green were calculated using IsoplotR (Vermeesch, 2018).

Four pre-unconformity Ovacık Group and Ulukışla Formation samples (11CAT05, 15, 16, and 17; Fig. 3) show AFT and AHe ages older than those in the western thrust nappe (above) but with a significant proportion of grain ages less than the minimum mid-Eocene stratigraphic age of these rocks, indicative of partial to full resetting of the AFT system following deposition (Fig. 13). In two of these samples, we were able to measure enough horizontal confined apatite fission-track lengths to model thermal histories most likely to predict our results (Fig. 14) using the inverse modeling software HeFTy version 1.9.3 (Ketcham, 2005; see Supplemental Material Methods Section [footnote 1] for details of HeFTy modeling methods and applied tT constraint boxes).

Best-fit thermal histories from both samples show similar very rapid postdepositional heating to temperatures >120 °C within 5–10 m.y. Given that the Paleogene sedimentary succession in the Ecemiş corridor is at least several kilometers thick, much of this heating can be attributed to sedimentary burial. However, at least part of this heating could also be related to structural burial beneath overriding thrust nappes during the stage 1 postdepositional shortening and transpression of these rocks (see section 4) or, for sample 11CAT05, elevated geothermal gradients related to volcanic rocks and/or pillow lavas observed within the Ulukışla Formation. Following maximum reheating, both samples then show rapid late Eocene cooling between ca. 45 and 35 Ma, followed by a period of slow cooling between ca. 35 Ma and 20 Ma, and in sample 11CAT05, a second phase of rapid early Miocene cooling at ca. 20 Ma, coeval with the rapid cooling recorded by the four Çamardı and Evliyatepe Formation samples closest to the Niğde Massif. Finally, no good-fit paths could be found in either sample without allowing a small degree of reheating in the Neogene. This can be attributed to burial by Çukurbağ and Burç formations (at least 1 km thick in places; Jaffey and Robertson, 2005), some of which must have since been removed by more recent erosion.

Finally, the AFT results from the Çukurbağ and Burç formations are all apparently not reset (all grain ages are older than the depositional age) and thus provide information on the provenance of the apatite grains. They show a similar pattern to the DZ U-Pb and dZFT results. West of the Ecemiş fault zone, AFT grain ages are between ca. 80 Ma and 35 Ma, reflecting a source from the Niğde Massif and/or Paleogene intrusive rocks within the Ulukışla basin. Some of the younger ca. 35–40 Ma AFT ages may also reflect recycled apatite from nearby Paleogene sedimentary rocks that record their Eocene burial and exhumation during our stage 1 deformation and highlighted in our HeFTy modeling above. Noteworthy is that there are no young ca. 20 Ma AFT ages closest to the Niğde Massif. This may reflect the relative scarcity of such grains within the sediments of the Çukurbağ and Burç formations, or that rocks containing these young AFT cooling

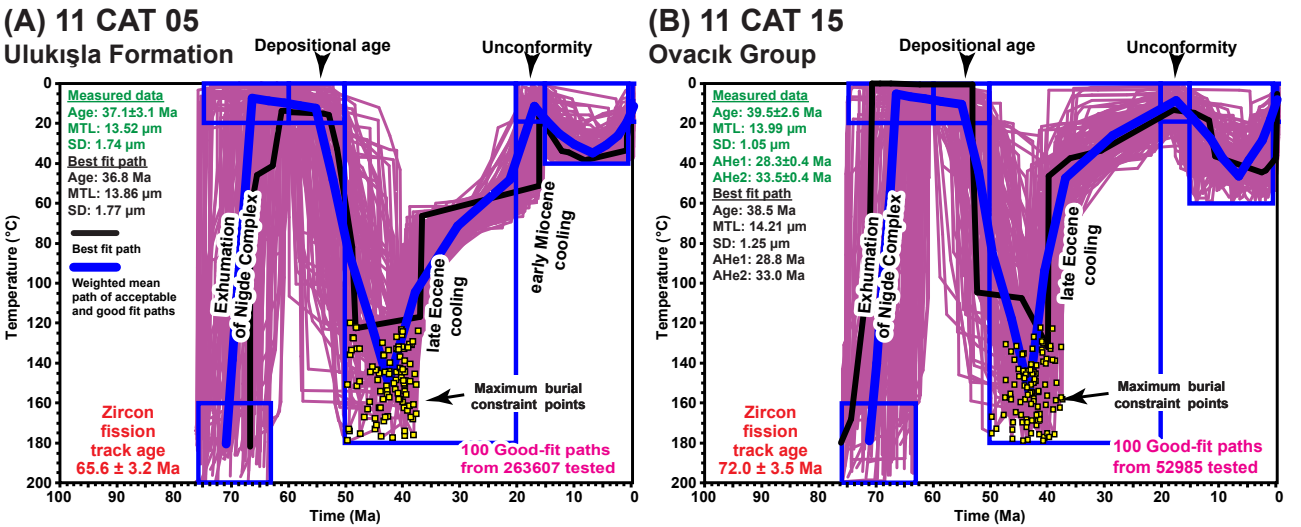

Figure 14. Results of HeFTy inverse time-temperature (tT) modeling based on apatite fission-track and (U-Th)/He data. For each sample, the first 100 good-fit tT paths are shown that best predict the measured data (see HeFTy modeling section in Supplemental Material for details on constraint boxes [text footnote 1]) methods for details on constraint boxes) along with the best-fit path (black) and weighted mean of acceptable and good-fit paths in blue. The predicted data for the best-fit path are shown along with the measured data for comparison. Inflection points for the tT paths are shown as yellow squares that highlight maximum postdeposition reheating allowed by the data.

ages were not yet exposed during deposition of the Çukurbağ Formation. Within the Ecemiş fault zone, apatite is scarce in our Çukurbağ Formation samples, reflecting their largely apatite-free ophiolitic and carbonate source areas. However, the detrital AFT ages we did obtain again reflect similar differences from west of versus within the Ecemiş fault zone as in our DZ U-Pb and dZFT data, with even a few older Mesozoic grains >100 Ma. Only in sample 11CAT13 was a significant proportion of young AFT grain ages of ca. 20 Ma obtained. Given that the DZ U-Pb and dZFT results show sediment in this sample was not derived from the Niğde Massif to the west, the source of these young detrital AFT grain ages is uncertain, but they may reflect early Miocene exhumational cooling within the Taurides.

6. DISCUSSION: CENOZOIC STRUCTURAL AND BASINAL HISTORY OF THE ECEMIŞ CORRIDOR AND REGIONAL IMPLICATIONS

This study results in a much clearer understanding of the Cenozoic structural history and basin development of the Ecemiş corridor and adjacent Ecemiş fault zone and Niğde Massif. Together with the recent study of the structural geology of the main Ulukışla basin to the south and west (Gürer et al., 2016), we have been able to reconstruct the co-evolution of basin formation and fault history from the Paleocene through the Miocene.

The southern Ulukışla basin has a record of Upper Cretaceous to middle Eocene marine strata that were deposited on Mesozoic ophiolite (Gürer et al., 2016). Variable extension occurred in the Late Cretaceous to Paleocene with late Paleocene volcanism of the Ulukışla Formation in the main Ulukışla basin to the south and along the Ecemiş corridor (this study). Marine deposition continued during a tectonically quiet period in the early to middle Eocene followed by major N-S shortening from late Eocene through much of Oligocene time (Gürer et al., 2016), equivalent to stage 1 transpression in the Ecemiş corridor documented in this study. The whole basin then underwent uplift and erosion, resulting in a major late Eocene to Oligocene unconformity. This was followed by formation of smaller subbasins filled with latest Oligocene to Miocene sedimentary deposits associated with stage 2 transtensional structures recognized in this study along and west of the left-lateral Ecemiş fault zone.

6.1. Stage 1: Late Eocene–Oligocene (ca. 45–40 to 25 Ma) Transpressional Stage

We identified three previously unrecognized major thrust faults that continue for at least 15–20 km along strike at the boundaries of the eastern Niğde Massif metamorphic belt and within the lower Cenozoic sedimentary and volcanic units immediately east of the massif (Figs. 3, 9, and 15). The thrust faults likely continue to the north along the same units but are covered by younger deposits or cut by the Ecemiş fault zone. The oblique nature of these thrust faults is supported by clear left-oblique top to the NNW kinematics at one location, and numerous secondary structures (cleavage, asymmetric folds, and reverse faults in Ovacık Group) between the thrust faults that consistently record NW to north vergence. A steeply plunging, recumbent fold at Kızılyusuftepe (~3 km SE of Çamardı; Figs. 3 and 5) indicates top-to-the-NE shortening. In other areas, conspicuous limestones suggest the presence of other thrust faults within the more poorly exposed parts of the Ulukışla Formation.

Our results strongly support top-to-the-NNW to north oblique kinematics on km-scale thrust faults that are subparallel to the main Ecemiş fault zone, consistent with generally north-south contraction observed on structures of late Eocene to Oligocene age in the greater Ulukışla basin (Gürer et al., 2016), but the role of the Ecemiş fault zone in this event remains uncertain. The lower Cenozoic units are fully involved in later deformation in the Ecemiş fault zone, which we argue is largely a Miocene and younger strike-slip fault zone in agreement with Jaffey and Robertson (2001). However, earlier left-oblique motion on the Ecemiş fault zone during the Eocene transpressional event, as suggested by Umhoefer et al. (2007), cannot be ruled out, although the sedimentology and provenance results from this study of the early Cenozoic units close to the Ecemiş fault zone suggest that no sediments were being sourced from the Taurides to the east at that time.

Thermochronological data from this study, and published data (Idleman et al., 2014), suggest that the Niğde Massif underwent a phase of burial in the Eocene related to sedimentary and/or structural burial, followed almost immediately by exhumation coeval with the oblique thrusting event documented here. This is the second stage of burial of the metamorphic rocks of the Niğde Massif and the first stage of burial of the lower Cenozoic sedimentary rocks in the yo-yo tectonics model of Umhoefer et al. (2007). The oblique thrust faults of this study provide a mechanism for both this burial event (structural burial in the footwall to these major thrust faults) and cooling of the Ulukışla Formation during thrust faulting related to erosion through creation of topographic relief. Partially reset AFT ages of Eocene sedimentary rocks immediately south of the Niğde Massif (11CAT15, 16, and 17) suggest that burial was more widespread here than current exposures demonstrate.

Anomalously young (apparently postdepositional) late Eocene (42–36 Ma) $^{40}Ar/^{39}Ar$ ages reported here from volcanic rocks within the Ulukışla Formation are coeval with the range of maximum burial temperatures at 45–40 Ma recorded by modeling of the AFT data (Fig. 14). The mechanism for the resetting of the younger $^{40}Ar/^{39}Ar$ ages is uncertain. If these samples are younger sills (rather than lava flows as they were interpreted in the field), this is problematic because there is little known magmatism at that time regionally (Schleiffarth et al., 2018). We suspect that hydrothermal processes and/or recrystallization in the upper crust during deformation may have reset the minerals during the thrusting event. We note that the $^{40}Ar/^{39}Ar$ spectra for the 42–36 Ma ages are not simple and suggest a complex thermal history. Also, the ZFT ages in all Eocene and younger samples show unreset detrital ages, which implies temperatures were not sufficient to reset the ZFT system (<~240 °C for radiation-damaged zircon for hold time >10 m.y.; Reiners and Brandon, 2006).

This favors the Ar ages having been reset by grain recrystallization during deformation, since even a very short-lived thermal event (<1 m.y.) would reset ZFT ages before $^{40}Ar/^{39}Ar$ in biotite (Reiners and Brandon, 2006, according to the experimentally determined biotite argon diffusion parameters of Grove and Harrison, 1996).

A major unconformity in the Ecemiş corridor from ca. 40–25 Ma marks the stratigraphic expression of the stage 1 transpressional deformation event and records a change from marine to terrestrial deposition (Fig. 15). The terrestrial Çukurbağ Formation lies unconformably over the marine Paleocene–Eocene units in many locations along the Ecemiş corridor. The locally strongly deformed Paleocene–Eocene units show a distinct contrast with the much less deformed Çukurbağ-Burç Formations. An exception to this pattern is locally strongly deformed rock of the Çukurbağ Formation affected by post-early Miocene strike-slip movement along the Ecemiş fault zone. Subsequent early to middle Miocene rapid cooling of the Paleogene units is coeval or slightly younger than deposition of the latest Oligocene–early Miocene Çukurbağ Formation.

In summary, our new mapping, along with structural and thermochronology data demonstrate that lower Cenozoic marine sedimentary rocks in the central to western Ecemiş corridor were thrust obliquely to the NNW to north over each other and over the Niğde Massif, and the eastern massif was thrust over the core of the massif, coeval with major N-S contraction in the southern Ulukışla basin (Gürer et al., 2016). This early transpressive deformation along the Ecemiş corridor suggests that the Ecemiş fault zone may have been a major strike-slip structure as early as the Eocene, but Miocene overprinting makes this difficult to demonstrate.

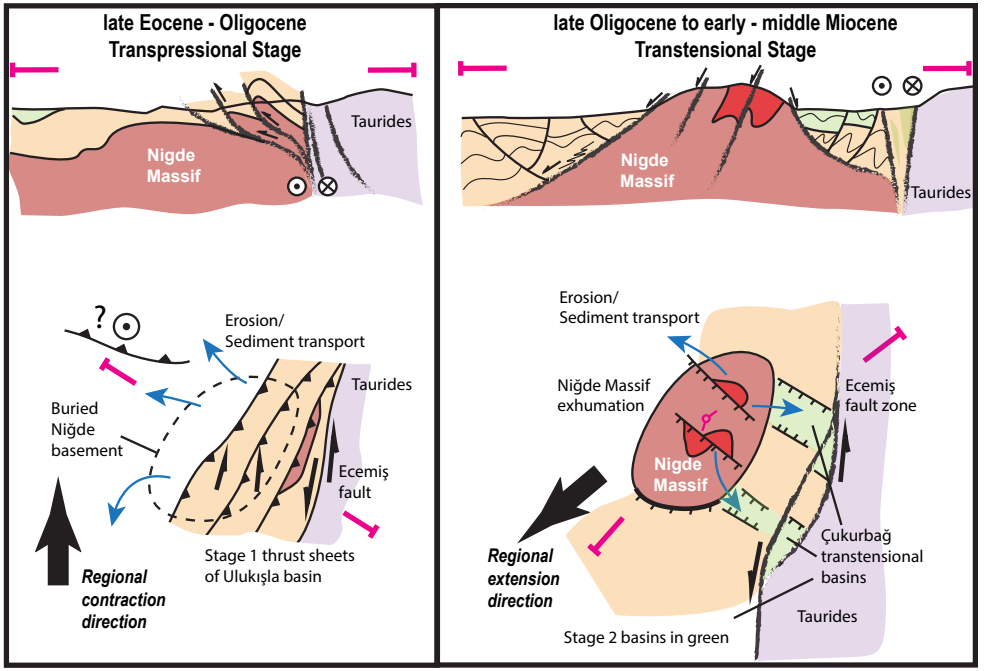

Figure 15. Schematic paleotectonic maps and cross sections of the study area for late Eocene to Oligocene transpressive-contractional stage 1 of deformation and early to middle Miocene stage 2 of transtensional to extensional deformation and proto-escape tectonics.

6.2. Stage 2: Latest Oligocene–Early Miocene (ca. 25–15 Ma) Transtensional Stage

A second stage of strike-slip and transtensional deformation affecting the sedimentary rocks of the Ecemiş corridor (Fig. 15) is well documented (Jaffey and Robertson, 2001; Umhoefer et al., 2007), but the timing was previously only known to postdate the oblique thrusting event recorded in the deformed Ovacık and Ulukışla Formations, owing to poor depositional age constraints of the terrestrial sediments of the Çukurbağ Formation. In this study, detrital zircon U-Pb dates from the Çukurbağ Formation constrain the maximum age of deposition as less than 22–23 Ma, supporting previous paleontology results (Yetiş, 1968) that show Burç Formation is Miocene in age. Here, we argue that the upper Çukurbağ Formation may correlate to the Burç Formation. The second episode of maximum burial and/or heating of the eastern Niğde Massif has been dated at ca. 30 ± 5 Ma by K-feldspar multi-domain diffusion modeling of metamorphic rocks at the eastern margin of the massif (Idleman et al., 2014). Following this burial episode, the final exhumation between ca. 25 and 15 Ma is recorded by our new AFT results, which include 19–20 Ma reset cooling ages from deformed Paleocene–Eocene rocks of the Çamardı Formation that nonconformably overlie metamorphic rocks of the Niğde Massif. Thermal modeling of partially reset AFT ages in the two samples from the Ovacık and Ulukışla units also indicate an early Miocene cooling event.

Deposition of the Çukurbağ and Burç formations after ca. 22–23 Ma is further supported by magnetostratigraphic results from the southern Ulukışla basin. These results show that the lower member of the Aktoprak Formation, the proposed lateral equivalent of the Çukurbağ Formation (Jaffey and Robertson, 2005), was deposited at 27.1–24.7 Ma (Meijers et al., 2016), and this is supported by Chattian–Aquitanian fossils (ca. 28–20 Ma) from the same formation (Nazik and Gökcen, 1992). Early

Miocene unroofing of a more extensive Paleocene–Eocene sedimentary cover above the Niğde Massif followed by mid-early Miocene unroofing and erosion of the massif rocks themselves is consistent with the lack of Miocene reset detrital AFT ages within our Çukurbağ Formation samples, as well as the absence of Niğde Massif–derived material in the lower, older parts of the Çukurbağ Formation (Jaffey and Robertson, 2005; Radwany et al., 2017). Conglomerates within the middle of the Çukurbağ Formation contain crystalline clasts sourced from the adjacent Niğde Massif; these clasts indicate the basement rocks of the massif were exposed and being eroded at the time of Çukurbağ Formation deposition in the early Miocene (younger than ca. 22–23 Ma). The youngest sedimentary rocks of the Ecemiş corridor include the upper Burç Formation, which in its type location has been interpreted based on gastropods to be middle to late Miocene in age (Yetiş, 1968). Cihanbeyli Formation rocks that unconformably overlie rocks of the Burç Formation are dated as late Miocene from 6 to 7 Ma tuffs (Meijers et al., 2018).

Our structural observations reveal that deformation in the Ecemiş corridor during and after deposition of the Çukurbağ Formation was dominated by left-lateral strike-slip faulting and related transtensional structures across the study area (Figs. 3 and 15). Note that virtually all the structures in the Pinarbaşı and Burç detailed study areas (Figs. 6 and 7) are compatible with left-lateral motion on the Ecemiş fault zone. The common presence of the Çukurbağ Formation within the Ecemiş fault zone strongly suggests that it was a topographically low belt along a transtensional fault zone, rather than a pure strike-slip fault with depocenters only at fault steps or bends. Local bends in faults within the Ecemiş fault zone facilitated the formation of mini-basins that were the site of the main deposition of the Çukurbağ Formation within the fault zone, while a long belt of Çukurbağ Formation was deposited immediately west of the fault zone (Fig. 3). The Çukurbağ and Burç formations are characterized structurally by open folds spaced ~500–1000 m apart that agree with left-lateral, strike-slip faulting on the Ecemiş fault zone with effects across the corridor (Figs. 3, 6, and 7), indicating that the Ecemiş fault zone continued as a strike-slip fault after deposition in the early to middle Miocene. Faults larger than a few meters of offset are rare in these local basins except near the Ecemiş fault zone.

All across the Ecemiş corridor, stage 1 transpressional structures are overprinted by stage 2 transtensional and extensional structures. The most prominent of these later structures is a group of northwest-southeast–striking normal faults that cut across the corridor and much of the Niğde Massif (Fig. 3). The orientation of these normal faults is compatible with left-lateral transtensional deformation on the Ecemiş fault zone. The Burç Formation basin is bounded by these normal faults. The eastern part of the southern boundary of the Niğde Massif is a south-dipping normal fault (Fig. 3), while the southern massif boundary to the west is poorly exposed.

A patch of Paleocene–Eocene–age Çamardı Formation, 1–3 km southwest of the city of Çamardı (Fig. 3), is deformed in a series of asymmetric, southwest-verging folds (Umhoefer et al., 2007) that we re-interpret to be related to southwest-dipping, moderate- to low-angle normal faults that link into a major normal fault that uplifts in its footwall both rocks of the Niğde Massif and the Çamardı Formation. All structural data from the Çamardı Formation along the southeast corner of the Niğde Massif indicate top-to-the-SSW faulting that we interpret as part of the transtensional stage of deformation. We note that an older oblique thrust fault is mapped on the southeastern edge of the patch of Çamardı Formation. This thrust fault likely formed during transpression and buried the rocks of the Çamardı Formation here, but the folds and normal faults that cut the formation are much more compatible with later transtensional deformation. The structures in the Çamardı Formation are similar to the two NW-striking, right-lateral (and down-to-the-south) oblique normal faults with ~150 and 100 m of separation that cuts the northeast limb of the Kızılyusuftepe syncline (Fig. 5).

Combined structural, sedimentological, and thermochronologic evidence from the Ecemiş corridor indicates that there was a major change in the tectonics of the area in the latest Oligocene to earliest Miocene, at ca. 25–22 Ma, to a transtensional stage of deformation. The distribution, sedimentology, and facies patterns of Çukurbağ and Burç formations in our study area and along the Ecemiş fault zone to the south (Jaffey and Robertson, 2005) suggest that these units were mainly deposited in separate transtensional basins within and up to ~5 km from the Ecemiş fault zone. Sedimentary evidence for local depocenters includes conglomerate clasts derived from multiple sides of each subbasin, lacustrine and laterally equivalent facies that suggest local lakes, paleocurrents from sandstones that indicate local inward draining basins (Jaffey and Robertson, 2005), small normal faults active during deposition, and the pattern of normal faults at a high angle to the Ecemiş fault zone that bound many of the basins.

6.3. Regional Implications for the Role and Age of the Ecemiş Fault Zone

Our results show that the Ecemiş fault zone has acted as a major tectonic boundary since at least the late Eocene and was characterized by two main phases of left-lateral strike-slip deformation. We identify an earlier stage 1 of transpression, uplift, and erosion during the late Eocene to Oligocene (ca. 45–25 Ma) and a stage 2 of transtension in the latest Oligocene to early middle Miocene (ca. 25–15 Ma). The first transpressional stage may be related to initial Eocene to Oligocene Africa/Arabia–Eurasia collision, as was interpreted for the onset of shortening in the Sivas Basin to the northeast across the Ecemiş fault zone (Darin et al., 2018). We interpret that the second latest Oligocene to Miocene stage of transtensional deformation is related to a "prototectonic escape" setting for central Anatolia west of the Ecemiş fault zone, possibly associated with cessation of final closure of southern Neotethys along the Bitlis suture (Şengör and Yılmaz, 1981; Okay et al., 2010; Cavazza et al., 2015, 2018) and increased extension in the Aegean region (Fig. 1) (Thomson et al., 1998; Jolivet et al., 2013; Faccenna et al., 2014).

The late Eocene–Oligocene cooling in the Ecemiş corridor is remarkably similar to the timing and

rates of cooling inferred from HeFTy modeling of AFT and AHe data from similar Paleogene marine sedimentary rocks within the nearby western Sivas Basin to the northwest (Darin et al., 2018). In both areas, we interpret this cooling phase as being related to structural basin inversion and erosional exhumation during initiation of major regional north-vergent shortening. In the southern Sivas fold-thrust belt, Darin et al. (2018) proposed that the shortening was related to initial soft collision of thinned continental crust of the Arabia plate with the Anatolide-Tauride block. We here interpret that the same Arabia soft collision was responsible for the stage 1 deformation in the Ecemiş corridor and initial left-lateral faulting along the Ecemiş fault zone. The apparently slightly earlier onset of cooling in our study area (ca. 45–35 Ma, compared to ca. 40–35 Ma in the western Sivas basin) also fits well with the general west to east propagation of initial deformation and exhumation recorded by thermochronologic results from the Sivas basin (Darin et al., 2018). This apparent common pre-Miocene depositional, structural, and exhumational history of the NE Ulukışla basin and western Sivas basin before formation of the regional late Eocene unconformity in both basins supports the idea that the basins once formed one continuous major retroforeland basin that became disconnected and offset by major Eocene to Miocene left-lateral displacement along the Ecemiş fault zone (Gürer et al., 2016; Darin et al., 2018).

The second transtensional stage includes a second stage of exhumation of deformed Eocene cover rocks of the Niğde Massif, deposition of the Çukurbağ and Burç formations in basins along the Ecemiş fault zone, and a major phase of left-lateral strike-slip faulting on the Ecemiş fault zone. New evidence presented here identifies at least 25 km of left-lateral displacement along the fault based on the offset of metamorphic rocks (Yahyalı metamorphic rocks) now found within the Ecemiş fault zone in the Emli-Kayacık Valley area. The major change from transpressional to transtensional deformation after 25–22 Ma was restricted to along and west of the Ecemiş fault zone and likely represents an early stage of the transition from collisional tectonics to escape tectonics across Anatolia.

7. CONCLUSIONS

New stratigraphic, geochronologic, and thermochronologic data presented here build on previous research in the Ulukisla Basin, allowing documentation of the significant changes in Cenozoic tectonic and sedimentary history between the Niğde Massif and the Ecemiş fault zone, or what we call the Ecemiş corridor. In particular, these data define the late Paleocene to middle Eocene Ulukışla Formation and overlying Ovacık Group, and the equivalent Çamardı and Evliyatepe formations in the Ecemiş corridor. The latter units overlie the basement rocks of the Niğde Massif with marginal to shallow marine environments, and the former units were a deeper marine sedimentary and volcanic setting within the Ecemiş corridor.

Structural data record a late Eocene–Oligocene transpressional deformation that included oblique northward thrusting of Paleogene strata and the eastern Niğde Massif onto the main massif. Left-lateral motion on the Ecemiş fault zone during this time is possible, but not well documented, and there was no input of sediments from the east. The timing and style of deformation in the Ecemiş corridor is similar to the same events in the Sivas basin to the northeast, which also restores nearly adjacent to the Ecemiş corridor across the Ecemiş fault zone. This regional contractional-transpressional event is interpreted to be caused by the soft collision of Arabia with Eurasia in the late Eocene to Oligocene.

A profound change in the tectonic setting at the end of the Oligocene produced a Miocene stage of transtensional deformation during which the Ecemiş fault zone had at least 25 km of left-lateral offset. During this faulting episode, the central Tauride Mountains to the east became a source of sediments into small transtensional terrestrial basins formed on the Eocene–Oligocene thrust belt between the Ecemiş fault zone and the Niğde Massif, another source of sediments. Normal faults compatible with regional SW-directed extension, and transtension along the Ecemiş fault zone, cut across the Niğde Massif, which exhumed during early to middle Miocene for a second time in the Cenozoic. Our new data show that the transtensional stage started at ca. 23–22 Ma, coeval with large changes across Anatolia in the early Miocene, and lasted until 15–10 Ma. These new results document the transition from collision to incipient-escape tectonics along and west of the Ecemiş fault zone as recorded at the western limit of deformation associated with the Arabia-Eurasia collision.

ACKNOWLEDGMENTS

This research was funded by National Science Foundation grant EAR-1109762, "Continental Dynamics: Central Anatolian Tectonics (CD-CAT)" to Whitney and Teyssier (University of Minnesota); EAR-1109336 to Thomson (University of Arizona); and EAR-1109826 to Umhoefer (Northern Arizona University). We thank Nuri Kaymakci, Daniel F. Stockli, Lauren Idleman, Erkan Toraman, Maud Meijers, Annia Fayon, Mike Darin, Kirk Schleiffarth, Ahmet Peynircioğlu, Noah Keller, and the whole CD-CAT team for many productive discussions. We thank the *Geosphere* editors and reviewers, and especially Megan Mueller for her thorough review. We thank Başar Şafak (Özşafak Pension in Çamardı) for his hospitality and friendship. Any use of trade, firm, or product names is for descriptive purposes only and does not imply endorsement by the U.S. Government.

REFERENCES CITED

Akıman, O., Erler, A., Göncüoğlu, M.C., Güleç, N., Geven, A., Türeli, T.K., and Kadıoğlu, Y.K., 1993, Geochemical characteristics of granitoids along the western margin of the Central Anatolian Crystalline Complex and their tectonic implications: Geological Journal, v. 28, p. 371–382, https://doi.org/10.1002/gj.3350280315.

Aydar, E., Gourgaud, A., Deniel, C., Lyberis, N., and Gundogdu, N., 1995, Quaternary Volcanism of Central Anatolia (Turkey): Association of Calc-Alkaline and Alkaline Magmatisms in a Zone of Convergence, Canadian Journal of Earth Sciences, v. 32, p. 1058–1069, https://doi.org/10.1139/e95-087.

Ballato, P., Parra, M., Schildgen, T.F., Dunkl, I., and Yıldırım, C., 2018, Multiple exhumation phases in the Central Pontides (N Turkey): New temporal constraints on major geodynamic changes associated with the closure of the Neo-Tethys Ocean: Tectonics, v. 37, p. 1831–1857, https://doi.org/10.1029/2017TC004808.

Candan, O., Akal, C., Koralay, O.E., Okay, A.I., Oberhänsli, R., Prelević, D., and Mertz-Kraus, R., 2016, Carboniferous granites on the northern margin of Gondwana, Anatolide-Tauride Block, Turkey—Evidence for southward subduction of Paleotethys: Tectonophysics, v. 683, p. 349–366, https://doi.org/10.1016/j.tecto.2016.06.030.

Cater, J.M.L., Hanna, S.S., Ries, A.C., and Turner, P., 1991, Tertiary evolution of the Sivas Basin, Central Turkey: Tectonophysics, v. 195, p. 29–46, https://doi.org/10.1016/0040-1951(91)90142-F.

Cavazza, W., Albino, I., Zattin, M., Galoyan, G., Imamverdiyev, N., and Melkonyan, R., 2015, Thermochronometric evidence for Miocene tectonic reactivation of the Sevan–Akera suture zone (Lesser Caucasus): A far-field tectonic effect of the Arabia–Eurasia collision?, *in* Sosson, M., Stephenson, R.A., and Adamia, S.A., eds., Tectonic Evolution of the Eastern Black

Sea and Caucasus: Geological Society of London Special Publication 428, no. 1, p. 187, https://doi.org/10.1144/SP428.4.
Cavazza, W., Cattò, S., Zattin, M., Okay, A.I., and Reiners, P., 2018, Thermochronology of the Miocene Arabia-Eurasia collision zone of southeastern Turkey: Geosphere, v. 14, p. 2277–2293, https://doi.org/10.1130/GES01637.1.
Chauvet, A., and Séranne, M., 1994, Extension-parallel folding in the Scandinavian Caledonides: Implications for late-orogenic processes: Tectonophysics, v. 238, p. 31–54, https://doi.org/10.1016/0040-1951(94)90048-5.
Clark, M., and Robertson, A., 2002, The role of the Early Tertiary Ulukışla Basin, southern Turkey, in suturing of the Mesozoic Tethys ocean: Journal of the Geological Society of London, v. 159, p. 673–690, https://doi.org/10.1144/0016-764902-015.
Clark, M., and Robertson, A., 2005, Uppermost Cretaceous–Lower Tertiary Ulukısla Basin, south-central Turkey: Sedimentary evolution of part of a unified basin complex within an evolving Neotethyan suture zone: Sedimentary Geology, v. 173, p. 15–51, https://doi.org/10.1016/j.sedgeo.2003.12.010.
Coleman, M.E., and Parrish, R.R., 1991, Eocene dextral strike-slip and extensional faulting in the Bridge River terrane, southwest British Columbia: Tectonics, v. 10, p. 1222–1238, https://doi.org/10.1029/91TC01078.
Cosentino, D., Schildgen, T.F., Cipollari, P., Faranda, C., Gliozzi, E., Hudácková, N., Lucifora, S., and Strecker, M.R., 2012, Late Miocene surface uplift of the southern margin of the central Anatolian Plateau, central Taurides, Turkey: Geological Society of America Bulletin, v. 124, p. 133–145, https://doi.org/10.1130/B30466.1.
Crowell, J.C., 1974, Origin of Late Cenozoic basins in southern California, *in* Dickenson, W.R., ed., Tectonics and Sedimentation: SEPM (Society for Sedimentary Geology), Special Publication 22, p. 190–204, https://doi.org/10.2110/pec.74.22.0190.
Darin, M.H., and Umhoefer, P.J., 2019, Structure and kinematic evolution of the southern Sivas fold-thrust belt, Sivas Basin, Central Anatolia, Turkey: Turkish Journal of Earth Sciences, v. 28, p. 834–859.
Darin, M.H., Umhoefer, P.J., and Thomson, S.N., 2018, Rapid late Eocene exhumation of the Sivas Basin (Central Anatolia) driven by initial Arabia-Eurasia collision: Tectonics, v. 37, p. 3805–3833, https://doi.org/10.1029/2017TC004954.
Dewey, J.F., and Strachan, R.A., 2003, Changing Silurian–Devonian relative plate motion in the Caledonides: sinistral transpression to sinistral transtension: Journal of the Geological Society of London, v. 160, p. 219–229, https://doi.org/10.1144/0016-764902-085.
Dhont, D., Chorowicz, J., Yurur, T., Froger, J.L., Kose, O., and Gündoğdu, N., 1998, Emplacement of volcanic vents and geodynamics of Central Anatolia, Turkey: Journal of Volcanology and Geothermal Research, v. 85, p. 33–54, https://doi.org/10.1016/S0377-0273(98)00048-1.
Dilek, Y., and Altunkaynak, S., 2009, Geochemical and temporal evolution of Cenozoic magmatism in western Turkey: Mantle response to collision, slab break-off, and lithospheric tearing in an orogenic belt, *in* van Hinsbergen, D.J.J., Edwards, M.A., and Govers, R., eds., Collision and Collapse at the Africa–Arabia–Eurasia Subduction Zone: Geological Society of London Special Publication 311, p. 213–233, https://doi.org/10.1144/SP311.8.
Dirik, K., Goncuoglu, M.C., and Kozlu, H., 1999, Stratigraphy and pre-Miocene tectonic evolution of the southwestern part of the Sivas Basin, Central Anatolia, Turkey: Geological Journal, v. 34, p. 303–319, https://doi.org/10.1002/(SICI)1099-1034(199907/09)34:3<303::AID-GJ829>3.0.CO;2-Z.
Ersoy, E.Y., and Palmer, M.R., 2013, Eocene-Quaternary magmatic activity in the Aegean: Implications for mantle metasomatism and magma genesis in an evolving orogeny: Lithos, v. 180–181, p. 5–24, https://doi.org/10.1016/j.lithos.2013.06.007.
Faccenna, C., Becker, T.W., Auer, L., Andrea Billi, A., Boschi, L., Brun, J.P., Capitanio, F.A., Funiciello, F., Horvàth, F., Jolivet, L., Piromallo, C., Royden, L., Rossetti, F., and Serpelloni, E., 2014, Mantle dynamics in the Mediterranean: Reviews of Geophysics, v. 52, p. 283–332, https://doi.org/10.1002/2013RG000444.
Fayon, A.K., Whitney, D.L., Teyssier, C., Garver, J.I., and Dilek, Y., 2001, Effects of plate convergence obliquity on timing and mechanisms of exhumation of a midcrustal terrain, the Central Anatolian Crystalline Complex: Earth and Planetary Science Letters, v. 192, p. 191–205, https://doi.org/10.1016/S0012-821X(01)00440-X.
Gabrielse, H., 1985, Major dextral transcurrent displacements along the northern Rocky Mountain trench and related lineaments in north-central British Columbia: Geological Society of America Bulletin, v. 96, p. 1–14, https://doi.org/10.1130/0016-7606(1985)96<1:MDTDAT>2.0.CO;2.
Gautier, P., Bozkurt, E., Hallot, E., and Dırık, K., 2002, Dating the exhumation of a metamorphic dome: geological evidence for pre-Eocene unroofing of the Niğde Massif (Central Anatolia, Turkey): Geological Magazine, v. 139, p. 559–576, https://doi.org/10.1017/S0016756802006751.
Gautier, P., Bozkurt, E., Bosse, V., Hallot, E., and Dirik, K., 2008, Coeval extensional shearing and lateral underflow during Late Cretaceous core complex development in the Niğde Massif, Central Anatolia, Turkey: Tectonics, v. 27, TC1003, https://doi.org/10.1029/2006TC002089.
Göncüoğlu, M.C., 1982, Niğde Masifinde paragnayslarinda zirkon U/Pb yaşlari: Türkiye Jeoloji Kurumu Bülteni, v. 25, p. 61–66.
Göncüoğlu, M.C., Toprak, V., Kuscu, I., Erler, A., and Olgun, E., 1991, Geology of the western part of the Central Anatolian Massif: Part 1, Southern section: Turkish Petroleum Corporation (TPAO) Report no. 2909, 140 p.
Grove, M., and Harrison, T.M., 1996, $^{40}Ar^{*}$ diffusion in Fe-rich biotite: The American Mineralogist, v. 81, p. 940–951, https://doi.org/10.2138/am-1996-7-816.
Gürer, D., van Hinsbergen, D.J.J., Matenco, L., Corfu, F., and Cascella, A., 2016, Kinematics of a former oceanic plate of the Neotethys revealed by deformation in the Ulukışla basin (Turkey): Tectonics, v. 35, p. 2385–2416, https://doi.org/10.1002/2016TC004206.
Gürer, D., van Hinsbergen, D.J., Özkaptan, M., Creton, I., Koymans, M.R., Cascella, A., and Langereis, C.G., 2018, Paleomagnetic constraints on the timing and distribution of Cenozoic rotations in central and eastern Anatolia: Solid Earth, v. 9, p. 295–322, https://doi.org/10.5194/se-9-295-2018.
Hempton, M., 1982, The North Anatolian fault and complexities of continental escape: Journal of Structural Geology, v. 4, p. 502–504, https://doi.org/10.1016/0191-8141(82)90041-4.
Hempton, M.R., 1987, Constraints on Arabian plate motion and extensional history of the Red Sea: Tectonics, v. 6, p. 687–705, https://doi.org/10.1029/TC006i006p00687.
Higgins, M., Schoenbohm, L.M., Brocard, G., Kaymakci, N., and Gosse, J.C., 2015, New kinematic and geochronologic evidence for the Quaternary evolution of the Central Anatolian fault zone (CAFZ): Tectonics, v. 34, p. 2118–2141, https://doi.org/10.1002/2015TC003864.
Idleman, L., Cosca, M.A., Thomson, S.N., Heizler, M.T., Teyssier, C., and Whitney, D.L., 2014, Tectonic burial and exhumation cycles tracked by muscovite and K-feldspar $^{40}Ar/^{39}Ar$ in a strike-slip fault zone, central Turkey: Tectonophysics, v. 612–613, p. 134–146, https://doi.org/10.1016/j.tecto.2013.12.003.
Jaffey, N., and Robertson, A.H.F., 2001, New sedimentological and structural data from the Ecemiş fault zone, southern Turkey: Implications for its timing and offset and the Cenozoic tectonic escape of Anatolia: Journal of the Geological Society of London, v. 58, p. 367–378, https://doi.org/10.1144/jgs.158.2.367.
Jaffey, N., and Robertson, A., 2005, Non-marine sedimentation associated with Oligocene–Recent exhumation and uplift of the Central Taurus Mountains, S Turkey: Sedimentary Geology, v. 173, p. 53–89, https://doi.org/10.1016/j.sedgeo.2003.11.025.
Jolivet, L., and Faccenna, C., 2000, Mediterranean extension and the Africa-Eurasia collision: Tectonics, v. 19, p. 1095–1106, https://doi.org/10.1029/2000TC900018.
Jolivet, L., Faccenna, C., Huet, B., Labrousse, L., Le Pourhiet, L., and Lacombe, O., 2013, Aegean tectonics: Strain localisation, slab tearing and trench retreat: Tectonophysics, v. 597, p. 1–33, https://doi.org/10.1016/j.tecto.2012.06.011.
Kaymakcı, N., Özçelik, Y., White, S.H., and Van Dijk, P.M., 2009, Tectono-stratigraphy of the Çankırı Basin: Late Cretaceous to early Miocene evolution of the Neotethyan suture zone in Turkey, *in* van Hinsbergen, D.J.J., Edwards, M.A., and Govers, R., eds., Collision and Collapse at the Africa-Arabia-Eurasia Subduction Zone: Geological Society of London Special Publication 311, p. 67–106, https://doi.org/10.1144/SP311.3.
Ketcham, R.A., 2005, Forward and inverse modeling of low-temperature thermochronometry data: Reviews in Mineralogy and Geochemistry, v. 58, p. 275–314, https://doi.org/10.2138/rmg.2005.58.11.
Koçyiğit, A., and Beyhan, A., 1998, A new intracontinental transcurrent structure; the central Anatolian fault zone, Turkey: Tectonophysics, v. 284, p. 317–336, https://doi.org/10.1016/S0040-1951(97)00176-5.
Köksal, S., Möller, A., Göncüoğlu, M.C., Frei, D., and Gerdes, A., 2011, Crustal homogenization revealed by U-Pb zircon ages and Hf isotope evidence from the Late Cretaceous granitoids of the Agaçören intrusive suite (Central Anatolia/Turkey): Contributions to Mineralogy and Petrology, v. 163, p. 725–743, https://doi.org/10.1007/s00410-011-0696-2.
Kusçu, I., Kuscu, G.G., Tosdal, R.M., Ulrich, T.D., and Friedman, R., 2010, Magmatism in the south astern Anatolia orogenic belt: Transition from arc to post-collisional setting in an evolving orogeny, *in* Sosson, M., Kaymakci, N., Stephenson, R.A., Bergerat, F., and Starostenko, V., eds., Sedimentary Basin Tectonics from the Black Sea and Caucasus to the Arabian Platform: Geological Society of London Special Publication 340, p. 437–460, https://doi.org/10.1144/SP340.19.
Le Pennec, J.L., Bourdier, J.L., Froger, J.L., Temel, A., Camus, G., and Gourgaud, A., 1994, Neogene ignimbrites of the Nevsehir plateau (central Turkey): Stratigraphy, distribution

and source constraints: Journal of Volcanology and Geothermal Research, v. 63, p. 59–87, https://doi.org/10.1016/0377-0273(94)90018-3.

Lüdecke, T., Mikes, T., Rojay, B., Cosca, M., and Mulch, A., 2013, Stable isotope reconstruction of Oligo-Miocene paleoenvironment and paleo-hydrology of Central Anatolian lake basins (Turkey): Turkish Journal of Earth Sciences, v. 22, p. 793–819, https://doi.org/10.3906/yer-1207-11.

McQuarrie, N., and van Hinsbergen, D.J., 2013, Retrodeforming the Arabia-Eurasia collision zone: Age of collision versus magnitude of continental subduction: Geology, v. 41, p. 315–318, https://doi.org/10.1130/G33591.1.

Meijers, M.J., Kaymakci, N., van Hinsbergen, D.J., Langereis, C.G., Stephenson, R.A., and Hippolyte, J.C., 2010, Late Cretaceous to Paleocene oroclinal bending in the central Pontides (Turkey): Lithos, v. 119, p. 412–426, https://doi.org/10.1016/j.lithos.2010.07.017.

Meijers, M.J., Brocard, G.Y., Cosca, M.A., Lüdecke, T., Teyssier, C., Whitney, D.L., and Mulch, A., 2018, Rapid late Miocene surface uplift of the central Anatolian Plateau margin: Earth and Planetary Science Letters, v. 497, p. 29–41, https://doi.org/10.1016/j.epsl.2018.05.040.

Meijers, M.J.M., Strauss, B.E., Özkaptan, M., Feinberg, J.M., Mulch, A., Whitney, D.L., and Kaymakçi, N., 2016, Age and paleoenvironmental reconstruction of partially remagnetized lacustrine sedimentary rocks (Oligocene Aktoprak basin, central Anatolia, Turkey): Geochemistry, Geophysics, Geosystems, v. 17, p. 914–939, https://doi.org/10.1002/2015GC006209.

MTA (General Directorate of Mineral Research and Exploration), 2002, 1:500,000-Scale Geological Maps of Turkey: Ankara, Turkey: General Directorate of Mineral Research and Exploration (MTA), scale 1:500,000.

Nazik, A., and Gökcen, N., 1992, Ostracoda genus Zonocypris and its species in Kurtulmuş Formation of Ulukışla Basin (Turkey): Rev. Esp. Micropaleontology, v. 24, p. 63–69.

Okay, A.I., and Tüysüz, O., 1999, Tethyan sutures of northern Turkey, *in* Mascle, A., and Jolivet, L., eds., The Mediterranean Basins: Tertiary Extension within the Alpine Orogeny: Geological Society of London Special Publication 156, p. 475–516.

Okay, A.I., Zattin, M., and Cavazza, W., 2010, Apatite fission-track data for the Miocene Arabia-Eurasia collision: Geology, v. 38, p. 35–38, https://doi.org/10.1130/G30234.1.

Parlak, O., Karaoğlan, F., Rizaoğlu, T., Klötzli, U., Koller, F., and Billor, Z., 2013, U-Pb and ^{40}Ar-^{39}Ar geochronology of the ophiolites and granitoids from the Tauride belt: Implications for the evolution of the Inner Tauride suture: Journal of Geodynamics, v. 65, p. 22–37, https://doi.org/10.1016/j.jog.2012.06.012.

Peltzer, G., and Tapponnier, P., 1988, Formation and evolution of strike-slip faults, rifts, and basins during India-Asia collision: An experimental approach: Journal of Geophysical Research, v. 93, p. 15,085–15,117, https://doi.org/10.1029/JB093iB12p15085.

Pourteau, A., Candan, O., and Oberhänsli, R., 2010, High-pressure metasediments in central Turkey: Constraints on the Neotethyan closure history: Tectonics, v. 29, TC5004, https://doi.org/10.1029/2009TC002650.

Radwany, M., Whitney, D.L., Brocard, G., Umhoefer, P.J., and Teyssier, C., 2017, Ophiolite gabbro from source to sink: A record of tectonic and surface processes in Central Anatolia: Geosphere, v. 13, p. 1329–1358, https://doi.org/10.1130/GES01465.1.

Radwany, M.R., Morgan, L., and Whitney, D.L., 2020, Conditions, mechanisms, and timing of high-grade metamorphism and ductile deformation of the southern segment of the Central Anatolian Ophiolite: International Journal of Earth Sciences, https://doi.org/10.1007/s00531-020-01908-7.

Ratschbacher, L., Frisch, W., Linzer, H.G., and Merle, O., 1991, Lateral extrusion in the Eastern Alps, 2. Structural analysis: Tectonics, v. 10, p. 257–271, https://doi.org/10.1029/90TC02623.

Reid, M.R., Schleiffarth, W.K., Cosca, M.A., Delph, J.R., Blichert-Toft, J., and Cooper, K.M., 2017, Shallow melting of MORB-like mantle under hot continental lithosphere, Central Anatolia: Geochemistry, Geophysics, Geosystems, v. 18, p. 1866–1888, https://doi.org/10.1002/2016GC006772.

Reilinger, R., McClusky, S., Vernant, P., Lawrence, S., Ergintav, S., Cakmak, R., Ozener, H., Kadirov, F., Guliev, I., Stepanyan, R., Nadariya, M., Hahubia, G., Mahmoud, S., Sakr, K., ArRajehi, A., Paradissis, D., Al-Aydrus, A., Prilepin, M., Guseva, T., Evren, E., Dmitrotsa, A., Filikov, S.V., Gomez, F., Al-Ghazzi, R., and Karam, G., 2006, GPS constraints on continental deformation in the Africa-Arabia-Eurasia continental collision zone and implications for the dynamics of plate interactions: Journal of Geophysical Research. Solid Earth, v. 111, B05411, https://doi.org/10.1029/2005JB004051.

Reiners, P.W., and Brandon, M.T., 2006, Using thermochronology to understand orogenic erosion: Annual Review of Earth and Planetary Sciences, v. 34, p. 419–466, https://doi.org/10.1146/annurev.earth.34.031405.125202.

Rolland, Y., Perincek, D., Kaymakci, N., Sosson, M., Barrier, E., and Avagyan, A., 2012, Evidence for ~80–75 Ma subduction jump during Anatolide-Tauride-Armenian block accretion and ~48 Ma Arabia-Eurasia collision in Lesser Caucasus–East Anatolia: Journal of Geodynamics, v. 56, p. 76–85, https://doi.org/10.1016/j.jog.2011.08.006.

Rubatto, D., Regis, D., Hermann, J., Boston, K., Engi, M., Beltrando, M., and McAlpine, S.R.B., 2011, Yo-yo subduction recorded by accessory minerals in the Italian Western Alps: Nature Geoscience, v. 4, p. 338–342, https://doi.org/10.1038/ngeo1124.

Schildgen, T.F., Cosentino, D., Bookhagen, B., Niedermann, S., Yıldırım, C., Echtler, H., Wittmann, H., and Strecker, M.R., 2012a, Multi-phased uplift of the southern margin of the Central Anatolian Plateau, Turkey: A record of tectonic and upper mantle processes: Earth and Planetary Science Letters, v. 317–318, p. 85–95, https://doi.org/10.1016/j.epsl.2011.12.003.

Schildgen, T.F., Cosentino, D., Caruso, A., Buchwaldt, R., Yıldırım, C., Bowring, S.A., Rojay, B., Echtler, H., and Strecker, M.R., 2012b, Surface expression of eastern Mediterranean slab dynamics: Neogene topographic and structural evolution of the southwest margin of the Central Anatolian Plateau, Turkey: Tectonics, v. 31, TC2005, https://doi.org/10.1029/2011TC003021.

Schleiffarth, W.K., Darin, M.H., Reid, M.R., and Umhoefer, P.J., 2018, Dynamics of episodic Late Cretaceous–Cenozoic magmatism across Central to Eastern Anatolia: New insights from an extensive geochronology compilation: Geosphere, v. 14, no. 5, p. 1990–2008, https://doi.org/10.1130/GES01647.1.

Selverstone, J., 1988, Evidence for east-west crustal extension in the eastern Alps: Implications for the unroofing history of the Tauern Window: Tectonics, v. 7, p. 87–105, https://doi.org/10.1029/TC007i001p00087.

Şengör, A.M.C., 1984, The Cimmeride Orogenic System and the Tectonics of Eurasia: Geological Society of America Special Paper 195, 74 p., https://doi.org/10.1130/SPE195-p1.

Şengör, A.M.C., and Yılmaz, Y., 1981, Tethyan evolution of Turkey: A plate tectonic approach: Tectonophysics, v. 75, p. 181–241, https://doi.org/10.1016/0040-1951(81)90275-4.

Sylvester, A.G., 1988, Strike-slip faults: Geological Society of America Bulletin, v. 100, p. 1666–1703, https://doi.org/10.1130/0016-7606(1988)100<1666:SSF>2.3.CO;2.

Temel, A., Gündoğdu, M.N., Gourgaud, A., and Le Pennec, J.L., 1998, Ignimbrites of Cappadocia (central Anatolia, Turkey): Petrology and geochemistry: Journal of Volcanology and Geothermal Research, v. 85, p. 447–471, https://doi.org/10.1016/S0377-0273(98)00066-3.

Thomson, S.N., Stöckhert, B., and Brix, M.R., 1998, Thermochronology of the high-pressure metamorphic rocks of Crete, Greece: Implications for the speed of tectonic processes: Geology, v. 26, p. 259–262, https://doi.org/10.1130/0091-7613(1998)026<0259:TOTHPM>2.3.CO;2.

Toprak, V., and Göncüoğlu, M.C., 1993, Tectonic control on the development of the Neogene–Quaternary Central Anatolian Volcanic Province, Turkey: Geological Journal, v. 28, p. 357–369, https://doi.org/10.1002/gj.3350280314.

Umhoefer, P.J., Whitney, D.L., Teyssier, C., Fayon, A.K., Casale, G., and Heizler, M.T., 2007, Yo-yo tectonics in a wrench zone, central Anatolia, *in* Till, A., Roeske, S., Sample, J., and Foster, D., eds., Exhumation and Continental Strike-Slip Fault Systems: Geological Society of America Special Paper 434, p. 35–57, https://doi.org/10.1130/2007.2434(03).

van Hinsbergen, D.J.J., Maffione, M., Plunder, A., Kaymakcı, N., Ganerød, M., Hendriks, B.W., Corfu, F., Gürer, D., de Gelder, G.I.N.O., Peters, K., McPhee, P.J., Brouwer, F.M., Advokaat, E.L., and Vissers, R.L.M., 2016, Tectonic evolution and paleogeography of the Kırşehir block and the Central Anatolian ophiolites, Turkey: Tectonics, v. 35, p. 983–1014 https://doi.org/10.1002/2015TC004018.

Vergili, Z., and Parlak, O., 2005, Geochemistry and tectonic setting of metamorphic sole rocks and mafic dikes from the Pinarbasi (Kayseri) Ophiolite, Central Anatolia (Turkey): Oflioliti, v. 30, p. 37–52.

Vermeesch, P., 2018, IsoplotR: A free and open toolbox for geochronology: Geoscience Frontiers, v. 9, p. 1479–1493, https://doi.org/10.1016/j.gsf.2018.04.001.

Whitney, D.L., and Dilek, Y., 1997, Core complex development in central Anatolia,Turkey: Geology, v. 25, p. 1023–1026, https://doi.org/10.1130/0091-7613(1997)025%3C1023:CCDICA%3E2.3.CO;2.

Whitney, D.L., and Dilek, Y., 1998, Metamorphism during crustal thickening and extension in central Anatolia: The Niğde metamorphic core complex: Journal of Petrology, v. 39, p. 1385–1403, https://doi.org/10.1093/petroj/39.7.1385.

Whitney, D.L., and Dilek, Y., 2001, Andalusite-sillimanite-quartz veins as indicators of low-pressure-high-temperature deformation during late-stage unroofing of a metamorphic core complex, Turkey: Journal of Metamorphic Geology, v. 18, p. 59–66, https://doi.org/10.1046/j.1525-1314.2000.00234.x.

Whitney, D.L., Teyssier, C., Dilek, Y., and Fayon, A.K., 2001, Metamorphism of the Central Anatolian Crystalline Complex, Turkey: influence of orogen-normal collision vs. wrench dominated tectonics on P-T-t paths: Journal of Metamorphic Geology, v. 19, p. 411–432, https://doi.org/10.1046/j.0263-4929.2001.00319.x.

Whitney, D.L., Teyssier, C., Fayon, A., Hamilton, M., and Heizler, M., 2003, Tectonic controls on metamorphism, partial melting, and intrusion: Timing and duration of regional metamorphism and magmatism in the Niğde Massif, Turkey: Tectonophysics, v. 376, p. 37–60, https://doi.org/10.1016/j.tecto.2003.08.009.

Whitney, D.L., Teyssier, C., and Heizler, M.T., 2007, Gneiss domes, metamorphic core complexes, and wrench zones: Thermal and structural evolution of the Niğde Massif, central Anatolia: Tectonics, v. 26, TC5002, https://doi.org/10.1029/2006TC002040.

Whitney, D.L., Umhoefer, P.J., Teyssier, C., and Fayon, A.K., 2008, Yo-yo tectonics of the Niğde Massif during wrenching in central Anatolia: Turkish Journal of Earth Sciences, v. 17, p. 209–217.

Wilcox, R.E., Harding, T.P., and Seely, D.R., 1973, Basic Wrench Tectonics: The American Association of Petroleum Geologists Bulletin, v. 57, p. 74–96.

Yalınız, M.K., Floyd, P.A., and Goncuoglu, M.C., 1996, Supra-subduction zone ophiolites of Central Anatolia: Geochemical evidence from the Sarikaraman Ophiolite, Aksaray, Turkey: Mineralogical Magazine, v. 60, p. 697–710, https://doi.org/10.1180/minmag.1996.060.402.01.

Yetiş, C., 1968, Geology of the Çamardı (Niğde) region and the characteristics of the Ecemiş Fault Zone between Maden Boğazi and Kamışlıç, Üniversitesi Fen Fak. Mecmuası: Seri B, v. 43, p. 41–61.

Yetiş, C., Kelling, G., Gökcen, S.L., and Baroz, F., 1995, A revised stratigraphic framework for Later Cenozoic sequences in the northeastern Mediterranean region: Geologische Rundschau, v. 84, p. 794–812, https://doi.org/10.1007/BF00240569.

Yıldırım, C., Sarıkaya, M.A., and Çiner, A., 2016, Late Pleistocene intraplate extension of the Central Anatolian Plateau, Turkey: Inferences from cosmogenic exposure dating of alluvial fan, landslide and moraine surfaces along the Ecemiş Fault Zone: Tectonics, v. 35, no. 6, p. 1446–1464, https://doi.org/10.1002/2015TC004038.

Yılmaz, Y., 1993, New evidence and model on the evolution of the southeast Anatolia orogeny: Geological Society of America Bulletin, v. 105, p. 251–271, https://doi.org/10.1130/0016-7606(1993)105<0251:NEAMOT>2.3.CO;2.

Yılmaz, Y., Tüysüz, O., Yiğitbas, E., Genç, Ş.C., and Sengör, A.M.C., 1997, Geology of tectonic evolution of the Pontides, *in* Robinson, A.G., ed., Regional and Petroleum Geology of the Black Sea and Surrounding Region: American Association of Petroleum Geologists Memoir 68, p. 183–226.

Yin, A., Rumelhart, P.E., Butler, R., Cowgill, E., Harrison, T.M., Foster, D.A., Ingersoll, R.V., Zhang, Q., Zhou, X.Q., Wang, X.F., Hanson, A., and Raza, A., 2002, Tectonic history of the Altyn Tagh fault system in northern Tibet inferred from Cenozoic sedimentation: Geological Society of America Bulletin, v. 114, p. 1257–1295, https://doi.org/10.1130/0016-7606(2002)114<1257:THOTAT>2.0.CO;2.